NOAA Technical Report NESDIS 143

Cross Track Infrared Sounder (CrIS) Sensor Data Record (SDR) User's Guide

Version 1.0

Washington, D.C.
December, 2013

U.S. DEPARTMENT OF COMMERCE
National Oceanic and Atmospheric Administration
National Environmental Satellite, Data, and Information Service

NOAA TECHNICAL REPORTS

National Environmental Satellite, Data, and Information Service

The National Environmental Satellite, Data, and Information Service (NESDIS) manages the Nation's civilian Earth-observing satellite systems, as well as global national data bases for meteorology, oceanography, geophysics, and solar-terrestrial sciences. From these sources, it develops and disseminates environmental data and information products critical to the protection of life and property, national defense, the national economy, energy development and distribution, global food supplies, and the development of natural resources.

Publication in the NOAA Technical Report series does not preclude later publication in scientific journals in expanded or modified form. The NESDIS series of NOAA Technical Reports is a continuation of the former NESS and EDIS series of NOAA Technical Reports and the NESC and EDS series of Environmental Science Services Administration (ESSA) Technical Reports.

An electronic copy of this report may be obtained at: https://cs.star.nesdis.noaa.gov/NCC/TBD

A limited number of copies of earlier reports are available by contacting, NOAA/NESDIS/STAR, 5830 University Research Ct, Suite 2600, College Park, Maryland 20740, Phone: 301 683-3490. A partial listing of more recent reports appears below:

NESDIS 111 **An Algorithm for Correction of Lunar Contamination in AMSU-A Data. Seiichiro Kigawa and Tsan Mo, December 2002.**

NESDIS 112 **Sampling Errors of the Global Mean Sea Level Derived from Topex/Poseidon Altimetry. Chang-Kou Tai and Carl Wagner, December 2002.**

NESDIS 113 **Proceedings of the International GODAR Review Meeting: Abstracts. Sponsors: Intergovernmental Oceanographic Commission, U.S. National Oceanic and Atmospheric Administration, and the European Community, May 2003.**

NESDIS 114 **Satellite Rainfall Estimation Over South America: Evaluation of Two Major Events. Daniel A. Vila, Roderick A. Scofield, Robert J. Kuligowski, and J. Clay Davenport, May 2003.**

NESDIS 115 **Imager and Sounder Radiance and Product Validations for the GOES-12 Science Test. Donald W. Hillger, Timothy J. Schmit, and Jamie M. Daniels, September 2003.**

NESDIS 116 **Microwave Humidity Sounder Calibration Algorithm. Tsan Mo and Kenneth Jarva, October 2004.**

NESDIS 117 **Building Profile Plankton Databases for Climate and EcoSystem Research. Sydney Levitus, Satoshi Sato, Catherine Maillard, Nick Mikhailov, Pat Cadwell, Harry Dooley, June 2005.**

NESDIS 118 **Simultaneous Nadir Overpasses for NOAA-6 to NOAA-17 Satellites from 1980 and 2003 for the Intersatellite Calibration of Radiometers. Changyong Cao, Pubu Ciren, August 2005.**

NESDIS 119 **Calibration and Validation of NOAA 18 Instruments. Fuzhong Weng and Tsan Mo, December 2005.**

NESDIS 120 **The NOAA/NESDIS/ORA Windsat Calibration/Validation Collocation Database. Laurence Connor, February 2006.**

NESDIS 121 **Calibration of the Advanced Microwave Sounding Unit-A Radiometer for METOP-A. Tsan Mo, August 2006.**

NESDIS 122 **JCSDA Community Radiative Transfer Model (CRTM). Yong Han, Paul van Delst, Quanhua Liu, Fuzhong Weng, Banghua Yan, Russ Treadon, and John Derber, December 2005.**

NESDIS 123 Comparing Two Sets of Noisy Measurements. Lawrence E. Flynn, April 2007.

NESDIS 124 Calibration of the Advanced Microwave Sounding Unit-A for NOAA-N'. Tsan Mo, September 2007.

NESDIS 125 The GOES-13 Science Test: Imager and Sounder Radiance and Product Validations. Donald W. Hillger and Timothy J. Schmit, September 2007.

NESDIS 126 A QA/QC Manual of the Cooperative Summary of the Day Processing System. William E. Angel, January 2008.

NESDIS 127 The Easter Freeze of April 2007: A Climatological Perspective and Assessment of Impacts and Services. Ray Wolf, Jay Lawrimore, April 2008.

NESDIS 128 Influence of the ozone and water vapor on the GOES Aerosol and Smoke Product (GASP) retrieval. Hai Zhang, Raymond Hoff, Kevin McCann, Pubu Ciren, Shobha Kondragunta, and Ana Prados, May 2008.

NESDIS 129 Calibration and Validation of NOAA-19 Instruments. Tsan Mo and Fuzhong Weng, editors, July 2009.

NESDIS 130 Calibration of the Advanced Microwave Sounding Unit-A Radiometer for METOP-B. Tsan Mo, August 2010.

NESDIS 131 The GOES-14 Science Test: Imager and Sounder Radiance and Product Validations. Donald W. Hillger and Timothy J. Schmit, August 2010.

NESDIS 132 Assessing Errors in Altimetric and Other Bathymetry Grids. Karen M. Marks and Walter H.F. Smith, January 2011.

NESDIS 133 The NOAA/NESDIS Near Real Time CrIS Channel Selection for Data Assimilation and Retrieval Purposes. Antonia Gambacorta and Chris Barnet, August 2011.

NESDIS 134 Report from the Workshop on Continuity of Earth Radiation Budget (CERB) Observations: Post-CERES Requirements. John J. Bates and Xuepeng Zhao, May 2011.

NESDIS 135 Averaging along-track altimeter data between crossover points onto the midpoint gird: Analytic formulas to describe the resolution and aliasing of the filtered results. Chang-Kou Tai, August 2011.

NESDIS 136 Separating the Standing and Net Traveling Spectral Components in the Zonal-Wavenumber and Frequency Spectra to Better Describe Propagating Features in Satellite Altimetry. Chang-Kou Tai, August 2011.

NESDIS 137 Water Vapor Eye Temperature vs. Tropical Cyclone Intensity. Roger B. Weldon, August 2011.

NESDIS 138 Changes in Tropical Cyclone Behavior Related to Changes in the Upper Air Environment. Roger B. Weldon, August 2011.

NESDIS 139 Computing Applications for Satellite Temperature Datasets: A Performance Evaluation of Graphics Processing Units. Timothy F.R. Burgess and Scott F. Heron, January 2011.

NESDIS 140 Microburst Nowcasting Applications of GOES. Ken Pryor, September 2011.

NESDIS 141 The GOES-15 Science Test: Imager and Sounder Radiance and Product Validations. Donald W. Hillger and Timothy J. Schmit, November 2011.

NOAA Technical Report NESDIS 143

Cross Track Infrared Sounder (CrIS) Sensor Data Record (SDR) User's Guide

Version 1.0

Yong Han[1], Yong Chen[2], Xin Jin[3], Denis Tremblay[4], Likun Wang[2]
[1]NOAA/NESDIS/STAR
College Park, MD 20740
[2] University of Maryland/ESSIC
College Park MD 20740
[3]ERT
Laurel, MD 20707
[4]Science Data Processing
Laurel, MD 20708

Washington, DC
December, 2013

U.S. DEPARTMENT OF COMMERCE
John Bryson, Secretary

National Oceanic and Atmospheric Administration
DR. Kathryn Sullivan, acting NOAA Administrator

National Environmental Satellite, Data, and Information Service
Mary Kicza, Assistant Administrator

Cross Track Infrared Sounder (CrIS) Sensor Data Record (SDR) User's Guide Version 1.0

Yong Han[1], Yong Chen[2], Xin Jin[3], Denis Tremblay[4], Likun Wang[2]

[1]NOAA/NESDIS/STAR, College Park, MD 20740
[2] ESSIC, College Park, MD 20740
[3]ERT, Laurel, MD 20707
[4]Science Data Processing Inc., Laurel, MD 20708

November 8, 2013

Revision Sheet

Revision	Date	Brief Summary of Changes
Version 1.0	November 8th, 2013	Baseline document

Note: For the latest versions of this document, please visit http://www.star.nesdis.noaa.gov/jpss/CrIS, or http://ncc.nesdis.noaa.gov in the CrIS section.

Table of Content

List of Figures

1. Introduction

The Cross-track Infrared Sounder (CrIS) is a Fourier Transform Spectrometer (FTS) onboard the Suomi National Polar-Orbiting Partnership (S-NPP) satellite, launched on October 28, 2011 into an orbit with an altitude of 824 km above the Earth surface, an inclination angle of 98.7^{o} and a 13:30 local time ascending node. S-NPP is the first in a series of next generation U.S. weather satellites of the Joint Polar Satellite System (JPSS). The CrIS system includes both the instrument and ground processing software. The instrument provides interferogram measurements and calibration data in the form of Raw Data Records (RDRs). The processing software converts the interferogram measurements into calibrated and geolocated radiance spectra in the form of Sensor Data Records (SDR).

The operational SDR data are produced by the Interface Data Processing Segment (IDPS) and are available to the public at the NOAA's Comprehensive Large Array-data Stewardship System (CLASS) (URL:
http://www.nsof.class.noaa.gov/saa/products/welcome
CrIS SDRs may also be produced by the Algorithm Development Library (ADL) software package. The ADL sofware includes the same CrIS SDR processing code and can run on multiple computing platforms including the Linux operating system. It provides a framework for algorithm and software development and refinement, bug fix and anomaly investigation. ADL uses file-based inputs and outputs, while IDPS uses a Data Management Subsystem (DMS) to manage the inputs and outputs.

This *CrIS Sensor Data Record User's Guide* (hereinafter referred to as the *User's Guide)* is intended for users of the S-NPP CrIS SDRs generated from the IDPS or ADL. It provides descriptions of SDR data fields, as well as some technical backgrounds to help understand the data. Many of the CrIS SDR as well as RDR data are trended and monitored with the web-based NOAA/STAR Integrated Calibration and Validation System (ICVS), open to public at:
http://www.star.nesdis.noaa.gov/icvs/status_NPP_CrIS.php
Detailed descriptions of the S-NPP CrIS SDR algorithms are given in the CrIS SDR Algorithm Theoretical Basis Document (ATBD) [JPSS Configuration Management Office, 2011a]. The S-NPP CrIS pre- and post-launch calibration and validation results are summarized in the peer-review papers by Han et al. [2013], Zavyalov et al. [2013], Stow et al. [2013], Tobin et al. [2013], Wang et al. [2013] and Chen et al. [2013].

2. Measurement Characteristics

The CrIS instrument provides interferogram measurements and calibration data, and the ground processing algorithms transform the interferograms into well calibrated and geolocated radiance spectra. In this section, the CrIS measurement characteristics are briefly described. The ground processing will be discussed in Section 3.

2.1 CrIS Interferograms

CrIS is a Michelson interferometer which measures interferograms in three Infrared (IR) bands simultaneously. The CrIS interferometer includes a beamsplitter, a porchswing moving mirror, a dynamic alignment (DA) mirror, and a laser metrology system. The incoming radiation is divided by the beamsplitter into two beams along two paths. One beam travels towards the porchswing mirror, while the other to the stationary mirror. The two beams are reflected from the corresponding mirrors and recombined at the beamsplitter. The optical path difference (OPD) between the two beams is twice the physical path difference between the two mirrors in vacuum. As the OPD changes with the sweep of the moving mirror, a time-varying interference pattern is produced by the interferometer. The DA mechanism on the stationary mirror maintains an active alignment between the two beams over the full path and therefore a stable modulation of the signal. The CrIS interferogram measurements are double-sided as shown in Figure 1 with the OPD varying from a negative Maximum Path Difference (MPD), through the Zero Path Difference (ZPD), to a positive MPD. The radiance coming from the interferometer is converged by the Telescope onto the long-wave IR (LWIR), mid-wave IR (MWIR) and short-wave IR (SWIR) detector focal planes with the use of dichroic splitters, which split the radiance beam into the three beams arriving at the three detector focal planes.

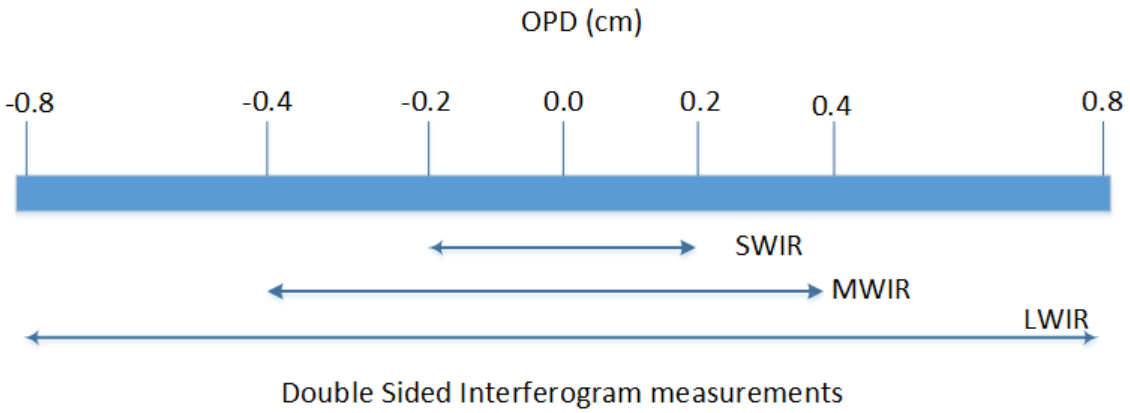

Figure 1 CrIS double sided interferogram measurements. The MWIR and SWIR OPDs are smaller than that of LWIR because the on-board processing truncates the interferograms of these two frequency bands. Planned for the near future is that the full resolution RDR will be downloaded on the ground where all interferogram maximum OPD will be 0.8 cm, which could be truncated to the current lengths during the ground operational processing.

The interferograms are sampled by 14-bit analog-to-digital (AD) converters that are triggered by the electrical pulses provided by a laser metrology system. This system injects a laser beam into the center of the interferometer optical path. Metrology detectors convert the modulated laser fringes into electrical pulses used as interferogram sampling signals. As the laser wavelength may vary with time, a neon metrology system provides periodic precise measurements of the laser wavelength using spectrally ultra

stable neon emission lines. The light from the neon lamp is injected in the same interferometer optical path as the metrology laser to generate the neon fringes. During a sweep interferogram measurement, counters are used to determine the number of fringes from both the metrology laser and neon lamp and the recorded data are used to determine the laser wavelength through a process of counting and interpolating neon fringes relative to the laser. The neon data set is generated roughly once per orbit.

The digitized interferogram measurements are further band limited by a complex Finite Impulse Response (FIR) digital filter, in addition to the pre-detection optical filtering. During the filtering process, the interferograms are also decimated in order to reduce the data size. Since the complex FIR filter is designed to have no image pass band, the decimation factors (DF) in use are twice as large as those a real-number filter can provide without having folding frequencies within the pass band. Table 1 lists the numbers of interferogram data points before and after the decimation, the decimation factor, and the values of the radiometric MPD. Figure 2 shows an example of the decimated interferogram for the LWIR Earth scene case.

Table 1 Current Interferogram characteristics.

Frequency Band	Number of samples before decimation	Effective OPD (cm)	Decimation Factor	Number of bins in the interferogram
LWIR	20738	0.8035	24	866
MWIR	10560	0.4092	20	530
SWIR	5200	0.2015	26	202

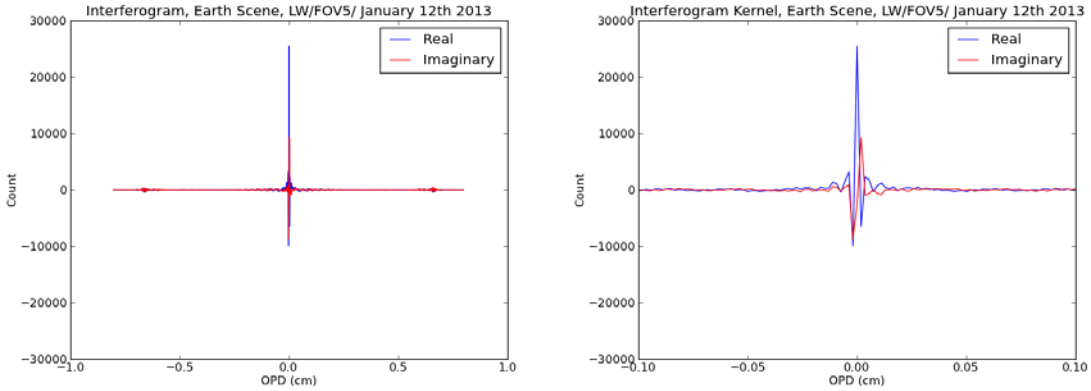

Figure 2 Example of a complex interferogram for LWIR showing all the points (left) and a zoom into its kernel (right) acquired on January 12th 2013.

For radiometric calibration, CrIS also provides measurements of two known radiation sources. One is the Internal Calibration Target (ICT), a high-precision calibration blackbody, and the other is the Deep Space (DS), a source with negligible IR radiance. The ICT temperature is measured with two high precision Platinum Resistance Thermometers (PRTs).

2.2 CrIS Field-OF-View, Field-OF-Regard and Scan Sequence

The Field-Of-Views (FOV) of the CrIS measurements are defined by the sizes and positions of the 9 detector field stops on each band focal planes, which are arranged into a 3x3 grid. The Field of Regard (FOR) is defined by the combined 3x3 FOVs. A typical sweep of the moving mirror produces a total of 27 interferograms from the 9 FOVs of a FOR and 3 spectral bands. A cross-track scan consists of 34 FORs, 30 of which are Earth scene (ES) views and 2 deep space (DS) views and 2 internal calibration target (ICT) views. The scan sequence is directed by the scene selection module with the upfront scanning mirror. It takes 8 seconds to acquire the entire scan. Figure 3 shows the cross-track scan sequence and Figure 4 depicts the concepts of the FOVs, FORs and scans.

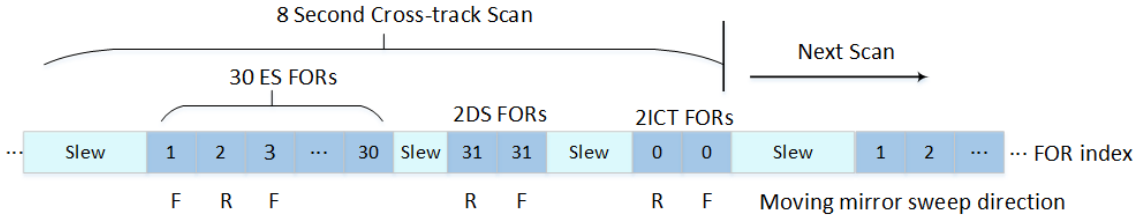

Figure 3 A cross-track scan sequence. F – forward direction; R – reverse direction.

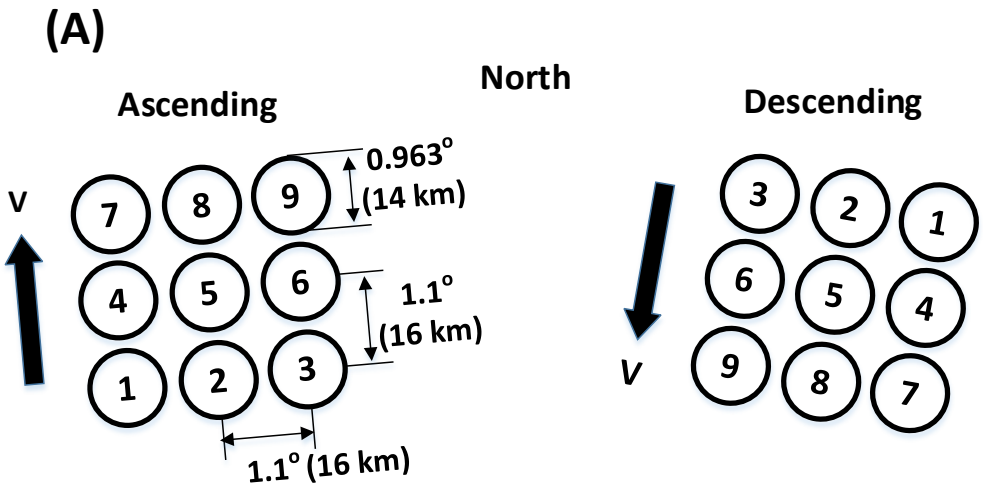

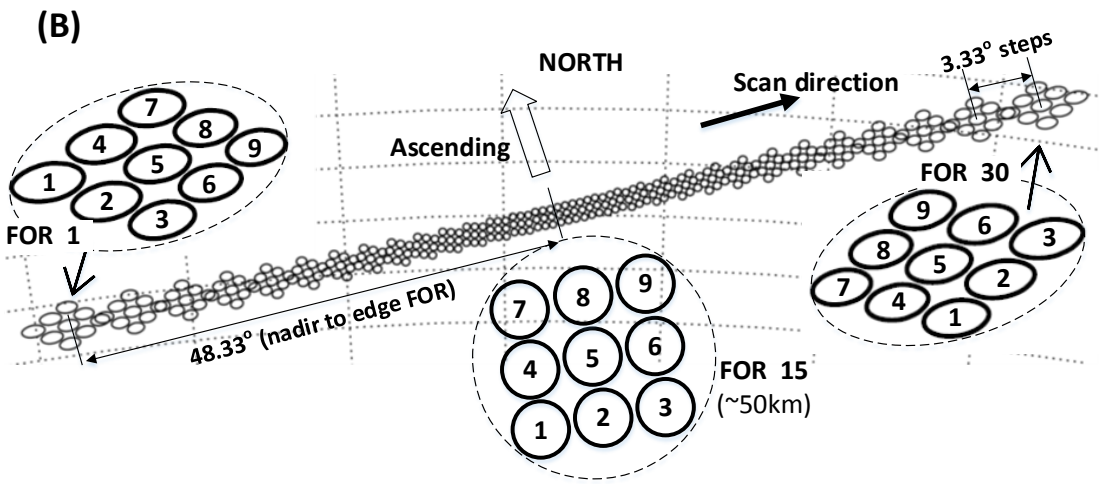

Figure 4 (A) CrIS footprints on Earth surface at nadir with FOV indexes viewed from the spacecraft on ascending (left) and descending orbits (right), respectively and (B) a typical scan viewed from an ascending orbit for FORs 1 to 30. V – spacecraft moving direction.

In a single day, CrIS acquires a total of 8.7 million spectra covering over 95% of the Earth surface. Figure 5 shows the geographical coverage of the CrIS Earth scene (ES) measurements during a single day accounting for the ascending and descending tracks.

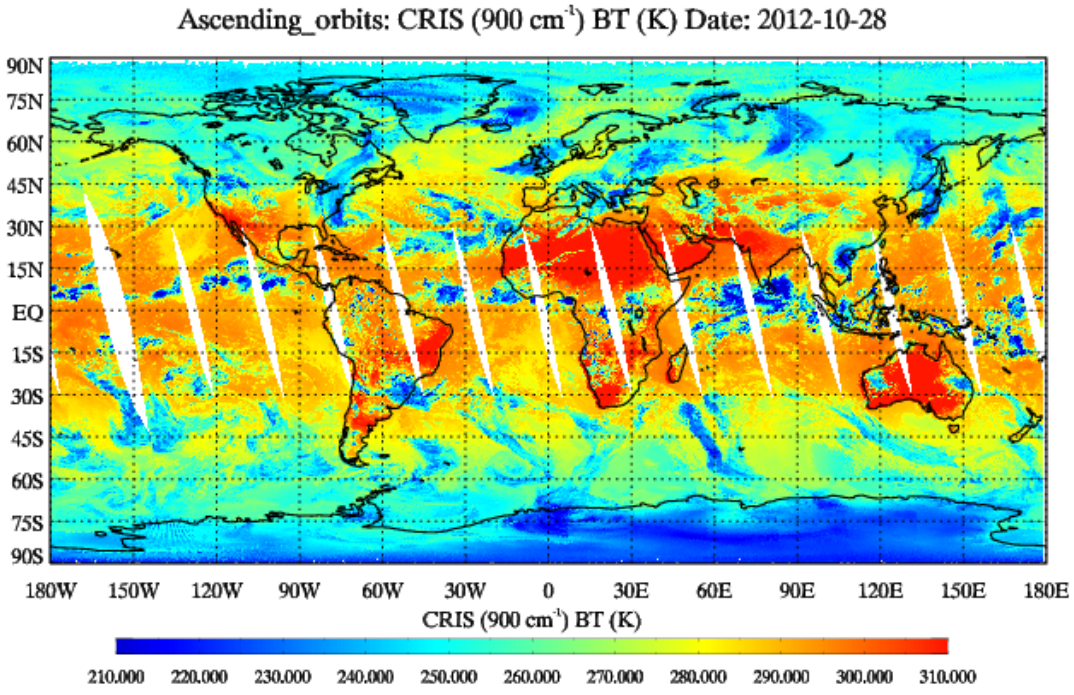

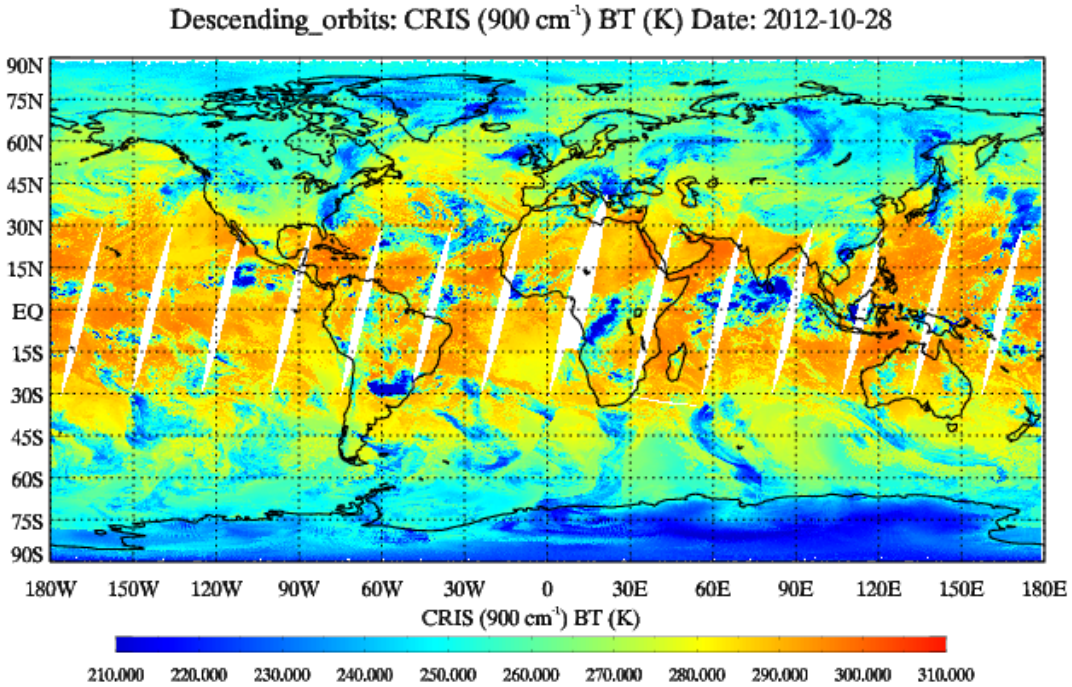

Figure 5 CrIS brightness temperature at 900 cm-1 showing the ascending (top) and descending (bottom) track geographical coverage for an entire day (Taken from the NOAA-STAR real time monitoring system web site).

2.3 CrIS Science Raw Data Record (RDR)

The data generated by the instrument are stored in various application packets in the form of RDRs, and the packets are broadcast from the Spacecraft to the ground receiving station. On the ground they are packed into RDR granules. The RDRs processed by the CrIS SDR algorithm are Science RDRs of three types: interferogram packet, 8-second science/calibration packet (SciCalP) and 4-minute Engineering packet (EP). An interferogram packet contains an ES, DS or ICT interferogram measurement. An 8-second SciCalP is created every 8 seconds for each scan. It contains calibration data such as ICT,andscan baffle temperature measurements. A 4-minute EP is created every 4 minutes, or after every 30 measurement scans. It includes calibration parameters and tables (e.g. ICT emissivity table), the neon metrology measurements, and the bit trim mask. The calibration parameters and tables are static and require an EP upload to change their content. The neon data are measurements taken roughly once per orbit and are automatically injected into EPs in space. A special feature of the CrIS calibration data set is that all the CrIS calibration parameters and tables are included in EPs, which are embedded in the data stream. A granule usually includes four scans of interferogram RDR packets, four corresponding SciCalPs and one or no EP.

3. SDR Processing Overview

3.1 SDR Processing Algorithms

CrIS SDR algorithms transform the interferograms into calibrated and geolocated Earth scene radiance spectra. The CrIS SDR ATBD contains detailed description of the data processing. The major computational steps are shown in Figure 6 and summarized below.

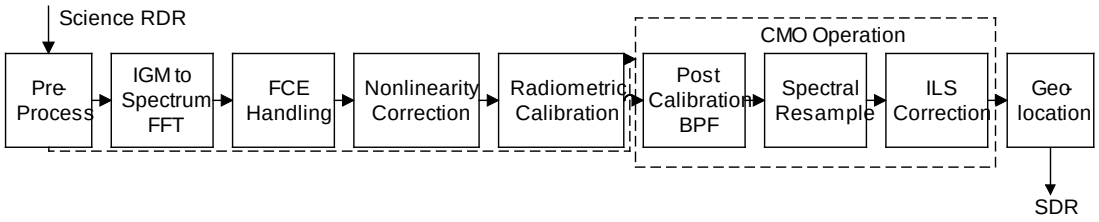

Figure 6 CrIS SDR processing flow.

1) Preprocess the input Science RDR data by unpacking the RDR granules and application packets, performing quality control tests and establishing a four-minute moving window for averaging DS and ICT data. The interferograms are decompressed according to the bit trim mask.
2) Transform (Fast Fourier Transform) the interferograms into raw spectra for all ES, DS and ICT views.
3) Perform the fringe count error (FCE) detection and correction. A FCE is an offset of the OPD leading to a linear change of phase in the raw spectrum. At the time of writing, the FCE algorithm is found to be defective and has been turned off since the beginning of the mission. This operation leads to a sampling phase alignment for the calibration view raw spectra of the same type. Should an FCE occur, the 'imaginary part' should detect it and flag the spectrum as invalid.
4) Perform nonlinearity correction for those detectors with significant nonlinearity. All the correction parameters are included in the engineering packet using the a2 and DC voltages.
5) Detect DS view lunar intrusion in the 4-minute moving window and once an intrusion is detected, remove the DS spectrum from the set of DS spectra for radiometric calibration.
6) Perform the radiometric calibration. This calculation removes the instrument offset and response function effects on the ES.
7) Calculate the noise for each spectral channel as the standard deviation of the calibrated ICT channel radiance, referred as Noise Equivalent Differential Radiance (NEdN).
8) Perform the various instrumental corrections. The so-called Correction Matrix Operation is a matrix that multiplies the spectrum calculated in the previous step. It

comprises a post calibration filter (removal of band edge effects), the correction of the Instrument line shape (ILS), correction of the residual ILS function, and resampling from the measured laser frequency grid into a common user grid.

9) Calculate the geolocation. The geolocation is the latitude and longitude of the FOV center on the Earth ellipsoid surface. It is not terrain corrected for the local altitude.

3.2 SDR Data Files

The CrIS SDR data are included in two separate data files (It may be combined into a single file in the ADL runs). The radiance data and associated quality description data are contained in the radiance data files and the corresponding geolocation data are contained in the geolocation data files. Both of the radiance and geolocation data files are provided to the users in the HDF 5 format. The data files also contain data quality flags, data quality indicators and the metadata.

A nominal (single granule) file contains 4 scans, measured in 32 seconds of observation time. About once per 4 days, a file will consist of a so-called short granule where there are 3 valid scans and the fourth scan is filled with fill values. This 4th scan does not correspond to any measurements.

3.2.1 Radiance Data File Naming Convention

The naming convention of IDPS operational SDR data file is specified as following:

SCRIS_npp_dYYYYMMDD_tHHmmSSS_eHHmmSSS_bXXXXX_cYYYYMMDDHHmmSSSSSSS_noaa_ops.h5

In the above file name, 'd*YYYYMMDD*' and tHHmmSSS are the observation date and time of the first FOR of the first scan in this data file, where *YYYY, MM, DD, HH, mm* and *SSS* are, respectively, the year (four digits), month (two digits), day (two digits), hour (two digits), minute (two digits) and second (three digits – the first two digits give the regular sexagesimal or base-60 second and the third digit gives the number of 0.1 seconds). The time '*HHmmSSS*' right after '_e' is the observation time of the last FOR of the last scan in this data file. The number '*XXXXX*' right after '_b' is the five-digit orbit ID of the first scan in the data file. The date and time '*YYYYMMDDHHmmSSSSSSS*' right after '_c' is the creation time of this file in the order of four-digit year, two-digit month, two-digit date, two-digit hour, two-digit minute, and 8-digit micro-second. All of the time stamps on the file name are UTC time. The '_noaa_ops.h5' string indicates that this data file is a HDF5-formatted file created by NOAA operational program.

Note that the difference between the time displayed in eHHmmSS and tHHmmss should be exactly 29.8 seconds. There is 2.2 seconds of slew time and acquiring calibration spectra (ICT and DS) giving 32 seconds for acquiring 4 scans. The following is an example of SDR file name:

SCRIS_npp_d20130801_t0519299_e0519597_b09120_c20130801113842529938_noaa_ops.h5

From this file name, the user knows that it is a CrIS SDR data file produced by NOAA operational procedure. The observation time of the first FOR in the first scan is 05:19:29.9 UTC, August 1st, 2013 and the observation time of the last FOR in the last scan is 05:19:59.7 UTC, August 1st, 2013. The orbit ID of the first scan is #09120. This file was created at 11:38:42.529938 UTC, August 1st, 2013.

The following is a case showing what the file name looks like when there is a date change in between the first FOR of the first scan and the first FOR of the last scan in the file:

SCRIS_npp_d20130801_t2359539_e0000237_b09131_c20130802061900319466_noaa_ops.h5

The first FOR in the first scan of this data file is sampled at 23:59:53.9 UTC, August 01, 2013 and the last FOR in the last scan is sampled at 00:00:23.7 UTC, August 02, 2013.

Sometime the user may receive more than one data files whose time stamps in '_dYYYYMMDD', '_tHHmmSSS' and '_eHHmmSSS' strings are exactly the same, and differ only the file creation time in '_cYYYYMMDDHHmmSSSSSSS'. This could be caused by one of the following two reasons.

1) The RDR data file (granule) used in the creation of an early SDR version is corrupted. The IDPS operational system re-tasked this granule several hours later when a repaired version of the RDR data is available. In general, only one good repaired version is produced. Sometimes, the first repaired RDR granule is still incomplete, and therefore the second repaired RDR granule is produced. In such a case, the SDR file with the latest creation time is usually the best one. The following three SDR files are an example of such a case:

SCRIS_npp_d20130722_t0426579_e0427277_b08978_c20130722104204650488_noaa_ops.h5
SCRIS_npp_d20130722_t0426579_e0427277_b08978_c20130723202118443032_noaa_ops.h5
SCRIS_npp_d20130722_t0426579_e0427277_b08978_c20130723203052433861_noaa_ops.h5

2) The SDR granule is re-packed by another program. For example, the CrIS SDR files archived in NOAA Comprehensive Large Array-data Stewardship System (CLASS) are re-packed versions of the same data received from the NASA Government Resource for Algorithm Verification, Integration, Test and Evaluation (GRAVITE) system. In such a case, the science content of the granule is unchanged. The following

two granules show such a case. The first one is directly downloaded from GRAVITE (Government Resource for Algorithm Verification, Independent Test, and Evaluation), and the second one is grabbed from CLASS. Their creation time is slightly different but the contents are exactly the same.

GRAVITE:
SCRIS_npp_d20130802_t0000259_e0000557_b09131_c20130802061900328214_noaa_ops.h5
CLASS:
SCRIS_npp_d20130802_t0000259_e0000557_b09131_c20130802061900319466_noaa_ops.h5

Since the _d/_t/_e time stamp reflects the temporal information of the first and last FOR in each granule, sometimes it could produce incorrect values such as _d19580101, _t0000000 or _e0000000 if the filled value, i.e. -993, is assigned to the first or last FOR when the information for this FOR is missing or corrupted. In the CrIS SDR algorithm, the epoch of all time stamps starts from 00:00:00 UTC, January 01, 1958, and a time stamp of -993 means there is a -993 microsecond delay between the epoch and the sampling time.

3.2.2 Geolocation Data File Naming Convention

The naming convention of IDPS operational granule geolocation file is the following:

GCRSO_npp_dYYYYMMDD_tHHmmSSS_eHHmmSSS_bXXXXX_cYYYYMMDDHHmmSSSSSSS_noaa_ops.h5

The above file name differs from the SDR file name only in the first five characters. The creation time of SDR and geolocation could have a slight difference. It is because the SDR and geolocation files are created by different modules at different time.

3.2.3 Data Array Dimensions

Many of the CrIS SDR data fields are stored with data arrays in the data files. Table 2 shows the array dimension names (used in this document) and values. For example, the SDR data field that holds the CrIS LWIR band spectra is a four-dimensional array with the dimensions N_{scan} x N_{for} x N_{fov} x N_{lw}. The nominal number of granules per file is one.

Table 2 SDR data array dimension names and values.

Name	Value	Description
N_g	Aggregation dependent	number of granules
N_{scan}	N_g*4	number of scans
N_{for}	30	number of Earth FORs
N_{fov}	9	number of FOVs
N_{lw}	717	number of spectral bins or channels for the LWIR band
N_{mw}	437	number of spectral bins or channels for the MWIR band
N_{sw}	163	number of spectral bins or channels for the SWIR band
N_{dir}	2	number of moving mirror scan directions

3.2.4 Data Fill Values

For various reasons a data element may be filled with one of the fill values, depending on the data type. The fill values are summarized in Table 3.

Table 3 SDRdata fill values.

Data Type	Definition*	Fill Value	Data Type	Definition*	Fill Value
Unsigned 8-bit integer	NA	255	64-bit integer	NA	-999
	MISS	254		MISS	-998
	ERR	251		ERR	-995
	VDNE	249		VDNE	-993
Unsigned 16-bit integer	NA	65535	32-bit Float point	NA	-999.9
	MISS	65534		MISS	-999.8
	ERR	65531		ERR	-999.5
	VDNE	65529		VDNE	-999.3
16-bit integer	NA	-999	64-bit Float point	NA	-999.9
	MISS	-998		MISS	-999.8
	ERR	-995		ERR	-999.5
	VDNE	-993		VDNE	-999.3

*The definitions of the fill values are described below:
NA – The data element was not computed because it is not applicable to this situation
MISS – The input data to be processed is missing
ERR – The algorithm could not correctly process the data
VDNE – Value Does Not Exist: the data was not available – it is not missing, nor is any attempt made to calculate the data

4. Radiance Product and Data Quality Information

A CrIS SDR contains one or more (aggregated) granules of radiance spectra, geolocation data and data quality information. A SDR file also contains metadata, providing information on the creation of this data record. The Earth scene radiance product is described in Section 4.1. Section 4.2 is an overview of the data quality

information. Section 4.3 describes the data quality indicators and Section 4.4 describes the data quality flags. Section 4.5 summarizes the metadata information.

4.1 Radiance Spectra – ES_RealLW, ES_RealMW and ES_RealSW

The contents of the LWIR, MWIR and SWIR band radiance data fields are summarized below:

Data field: LWIR radiance spectrum
Name: ES_RealLW
Type: 32-bit floating point
Dimension: N_{scan} x N_{for} x N_{fov} x N_{lw} (= N_g*4 x 30 x 9 x 717)
Units: mW/(m^2.sr.cm^{-1})
Fill value: see Table 3

Data field: MWIR radiance spectrum
Name: ES_RealMW
Type: 32-bit floating point
Dimension: N_{scan} x N_{for} x N_{fov} x N_{mw} (= N_g*4 x 30 x 9 x 437)
Units: mW/(m^2.sr.cm^{-1})
Fill value: see Table 3

Data field: SWIR radiance spectrum
Name: ES_RealSW
Type: 32-bit floating point
Dimension: N_{scan} x N_{for} x N_{fov} x N_{sw} (= N_g*4 x 30 x 9 x 163)
Units: mW/(m^2.sr.cm^{-1})
Fill value: see Table 3

The SDR radiance spectra are the real part of the complex spectra output from the SDR algorithms. The spectra are unapodized. Table 4 shows the spectral resolution, range and number of channels in each of the three bands. Figure 7 shows an example of the LWIR, MWIR, and SWIR Earth scene spectra. The channel theoretical spectral response function (SRF) is an ideal Sinc function, as shown in Figure 8. The actual as-observed SRF has additional noise, ringing, and round-off errors.

Table 4 has the information to construct the frequency scale associated with the spectra. For example, the LWIR spectra has 717 data points ranging from 648.75 to 1096.75 cm^{-1} with a frequency increment of 0.625 cm^{-1}.

The user may apply an apodization function to apodize the spectra, utilizing the four extra channels. The Hamming apodization function is a reasonable and efficient function to use for CrIS because the channel SRF after the apodization has side-lobes less than 1% of the central lobe. The Hamming apodization may be performed in the spectral domain on a spectrum with a running mean of the three point smooth filter {a, 1-2a, a}, where a = 0.23.

Table 4 Spectral resolution, frequency range, number of channels of the SDR product radiance spectra (unapodized). The SDR specifications of the spectral range and number of channels are also shown.

		Unapodized Spectrum *		SDR Specification	
band	Resolution (cm^{-1})	Frequency range (cm^{-1})	Number of Channels	Spectral range (cm^{-1})	Number of Channels
LWIR	0.625	648.75 to 1096.25	717	650-1095	713
MWIR	1.25	1207.5 to 1752.5	437	1210-1750	433
SWIR	2.5	2150 to 2555	163	2155-2550	159

*SDR product contains only unapodized spectra

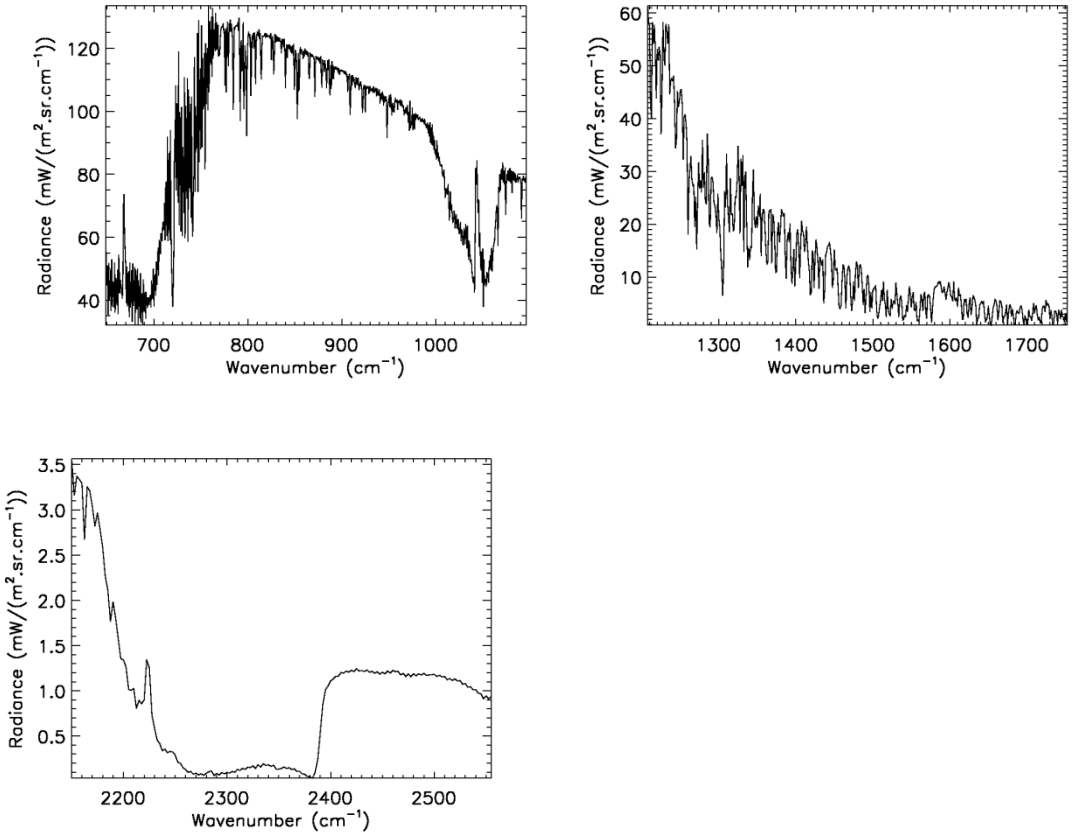

Figure 7 An example of Earth scene spectra in LWIR (top left), MWIR (top right) and SWIR (bottom) bands, at FOV5, FOR 15 acquired on July 29th 2013.

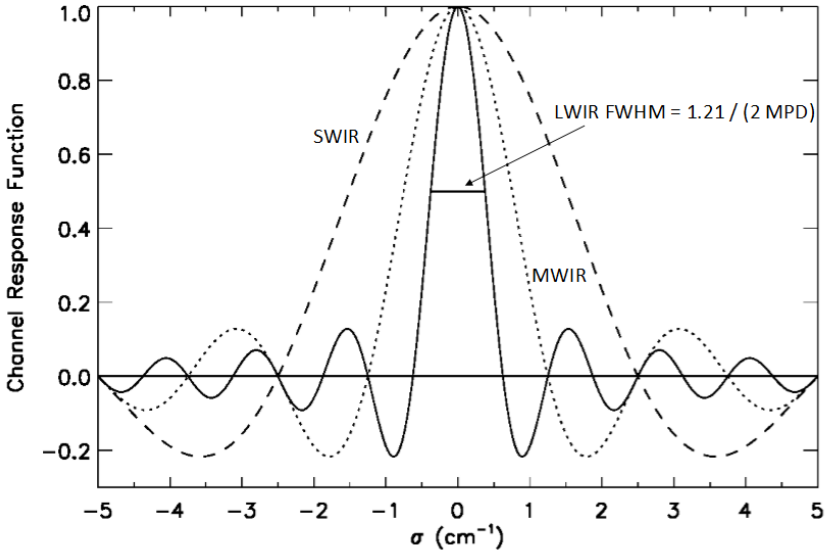

Figure 8 CrIS SDR channel spectral response functions of the LWIR (solid curve), MWIR (dotted curve) and SWIR (dashed curve) bands as a function of wavenumber. FWHM – Full Width at Half Maximum.

4.2 SDR Product Quality Information Overview

The CrIS SDR products provide several assessments of the quality of given spectra (the real parts of the complex spectra). The results of the assessments are included in two sets of SDR data fields, referred here as data quality indicators (DQI) and data quality flags (DQF).

A DQI is either a floating point value or an integer. A floating point value may describe a statistical assessment of a given parameter such as it is the case for the noise calculation (NEdN). The imaginary part of the spectrum is another example of a DQI. A DQI integer value may report the number of occurrences of a given condition. For example, the 30 internal calibration target (ICT) measurements are nominally averaged over 4 minutes forming the sliding window. The reported DQI named "ICT_WindowSize" is the actual number of ICT that are averaged. Table 5 has the list of the reported DQI. They are described in more details in Section 4.3.

Table 5 CrIS SDR data quality indicators.

Quality Variable Name(s)	Description
ES_ImaginaryLW, ES_ImaginaryMW, ES_ImaginarySW	LWIR, MWIR and SWIR imaginary radiance spectra
ES_NEdNLW, ES_NEdNMW, ES_NEdNSW	LWIR, MWIR and SWIR NEdN spectra
DS_WindowSize, ICT window size	DS and ICT Window Sizes
ES_ZPDAmplitude, ES_ZPDFringeCount	ES ZPD Amplitude and ES ZPD Fringe Count
SdrFringeCount	SDR Fringe Count
ES_RDRImpulseNoise	ES RDR Impulse Noise
MeasuredLaserWavelength, ResamplingLaserWavelength MonitoredLaserWavelength	Measured Laser Wavelength, Resampling Laser Wavelength and Monitored Laser Wavelength
DS_Symmetry	DS Symmetry
DS_SpectralStability, ICT_SpectralStability	DS and ICT Spectral Stability
ICT_TemperatureStability, ICT_TemperatureConsistency, NumberOfValidPRTTemps	ICT Temperature Stability, ICT Temperature Consistency and Number of Valid PRT Temperatures

A data quality flag (DQF) shows the status of a specified quality condition or state, which sets one or two specific bits in an 8-bit quality flag array. The four SDR flag byte arrays are shown in Table 6. The top-level DQF has dependency on DQI and/or other DQF as shown in Figure 9. Details of the DQF dependencies are presented in Section 4.4. Many DQF are named as “Invalid …” such as the ‘Invalid Geolocation” For this case, a value of zero indicates a ‘good’ geolocation quality whereas a value of 1 indicates an invalid geolocation calculation.

Table 6 CrIS SDR unsigned 8-bit integers which hold various quality flags, each taking no more than two bits.

Name	Description	Flags included
QF1_SCAN_CRISSDR	Scan-level Quality Flags	Data Gap flag Timing Sequence Error flag Lambda Monitored Quality flag Invalid Instrument Temperature flag Excess Thermal Drift flag Suspect Neon Calibration flag
QF2_CRISSDR	Lunar Intrusion Quality Flags	Lunar Intrusion Forward flag Lunar Intrusion Reverse flag
QF3_CRISSDR	Spectrum-level SDR Quality Flags	SDR Overall Quality flag* Invalid Geolocation flag Invalid Radiometric Calibration flag Invalid Spectral Calibration flag SDR Fringe Count Error Correction Failed flag
QF4_CRISSDR	Spectrum-level, some RDR Quality Flags Migrated to SDR	Day/Night Indicator flag Invalid RDR Data flag Fringe Count Error Detected flag Bit Trim Failed flag Imaginary Radiance Anomaly flag

*The SDR Overall Quality flag is a summary flag

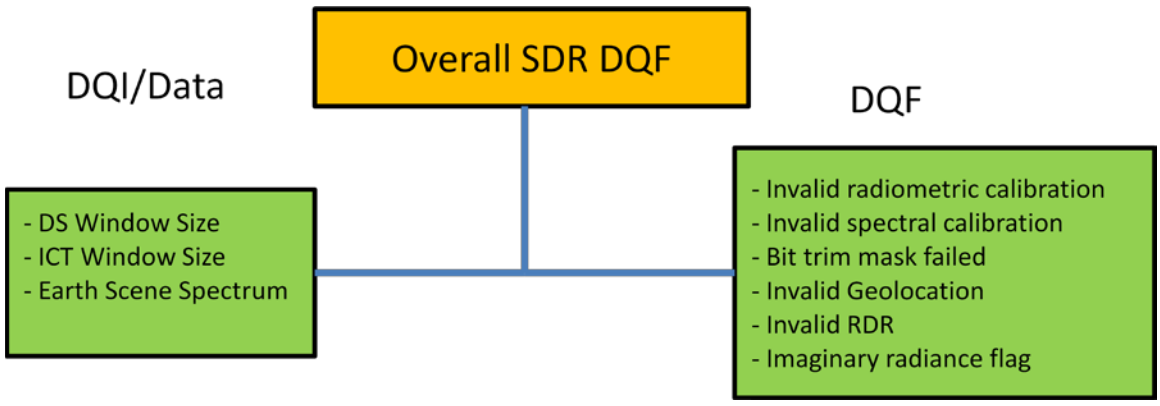

Figure 9 Schematic data quality flag tree structure showing dependency on data quality indicators (DQI) and/or other data quality flags (DQF).

4.3 Data Quality Indicators (DQI)

There are a total of 21 data quality indicators. Some of them are compared against threshold values which triggers the desired data quality flag. This section has details on the DQI, their array sizes, units, and formula.

4.3.1 Imaginary Radiance Spectra – ES_ImaginaryLW, ES_ImaginaryMW and ES_ImaginarySW

The contents of the imaginary part of the complex radiance data fields are summarized below:

Data field: LWIR imaginary radiance spectrum
Name: ES_ImaginaryLW
Type: 32-bit floating point
Dimension: N_{scan} x N_{for} x N_{fov} x N_{lw} (= N_g*4 x 30 x 9 x 717)
Units: mW/(m^2.sr.cm^{-1})
Fill value: see Table 3

Data field: MWIR imaginary radiance spectrum
Name: ES_ImaginaryMW
Type: 32-bit floating point
Dimension: N_{scan} x N_{for} x N_{fov} x N_{mw} (= N_g*4 x 30 x 9 x 437)
Units: mW/(m^2.sr.cm^{-1})
Fill value: see Table 3

Data field: SWIR imaginary radiance spectrum
Name: ES_ImaginarySW
Type: 32-bit floating point
Dimension: N_{scan} x N_{for} x N_{fov} x N_{sw} (= N_g*4 x 30 x 9 x 163)
Units: mW/(m^2.sr.cm^{-1})
Fill value: see Table 3

A Fourier Transform operation results in a real and imaginary spectral output. For ideal spectra with no noise, the radiometric calibration would result in a spectrum with the imaginary part of the radiance equal to zero for all channels. Large imaginary radiance is an indication of poor quality of the real part of the radiance. Note that the SDR imaginary radiance product is an output from the SDR algorithms before the CMO correction. In other words, the imaginary radiance spectra are in sensor spectral grids and are not corrected for self-apodization. An example of the LWIR, MWIR and SWIR imaginary radiance spectra is shown in Figure 10.

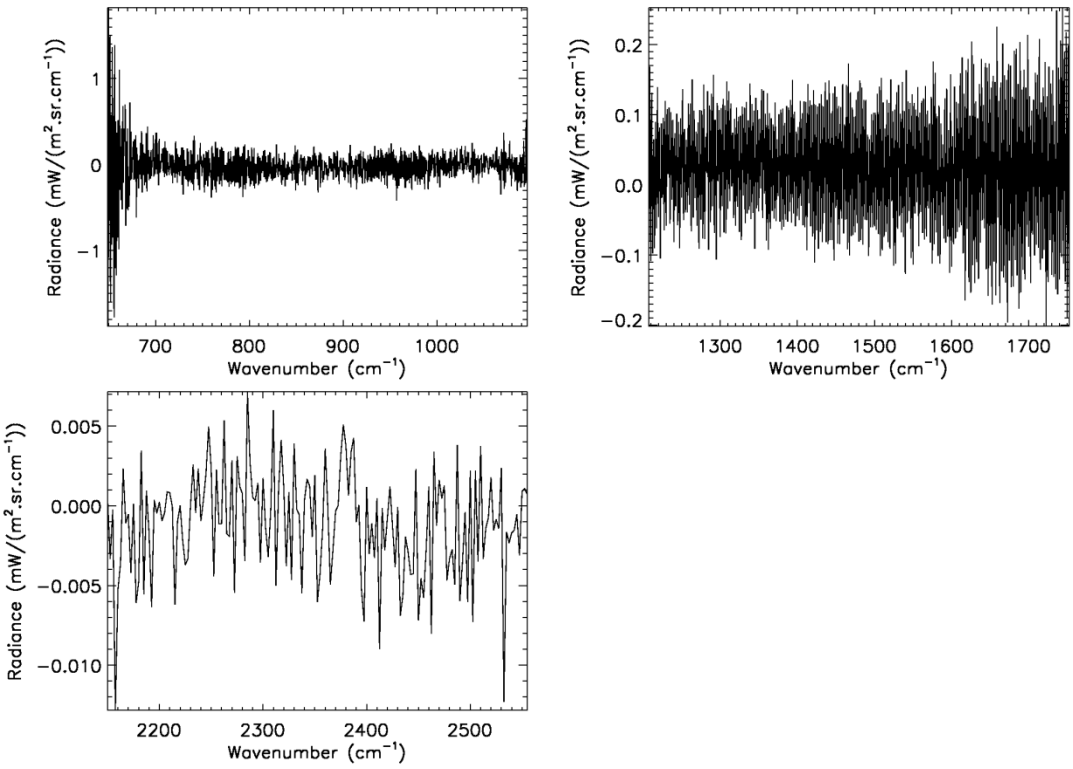

Figure 10 Example of Earth scene imaginary part of radiance spectra of LWIR (a), MWIR (b) and SWIR (c) bands, acquired on July 29th 2013, whose real part radiances are shown in Figure 7.

4.3.2 NEdN Spectra – ES_NEdNLW, ES_NEdNMW and ESNEdNSW

The contents of the NEdN data fields are summarized below:

Data field: LWIR NEdN spectrum
Name: ES_NEdNLW
Type: 32-bit floating point
Dimension: N_{scan} x N_{for} x N_{fov} x N_{lw} (= N_g*4 x 30 x 9 x 717)
Units: mW/(m^2.sr.cm^{-1})
Fill value: see Table 3

Data field: MWIR NEdN spectrum
Name: ES_NEdNMW
Type: 32-bit floating point
Dimension: N_{scan} x N_{for} x N_{fov} x N_{mw} (= N_g*4 x 30 x 9 x 437)
Units: mW/(m^2.sr.cm^{-1})
Fill value: see Table 3

Data field: SWIR NEdN spectrum
Name: ES_NEdNSW
Type: 32-bit floating point
Dimension: N_{scan} x N_{for} x N_{fov} x N_{sw} (= N_g*4 x 30 x 9 x 163)
Units: mW/(m^2.sr.cm^{-1})
Fill value: see Table 3

The forward (reverse) NEdN (Noise Equivalent Differential Radiance) spectrum is derived from calibrated ICT radiance spectra which are collected within the 4-minute moving window (30 ICT measurements) when the moving mirror moves in the forward (reverse) direction. The NEdN at a particular spectral bin is the standard deviation of the radiance ensemble at the same spectral bin. The NEdN estimate is smoothed over 17 adjacent spectral bins in the spectral domain in order to approximate it to that derived from a set of 512 data samples specified for NEdN calculation. Note that the same NEdN spectrum is populated in the NEdN data array along the N_{for} dimension. The typical NEdN spectra for CrIS three bands are shown in Figure 11.

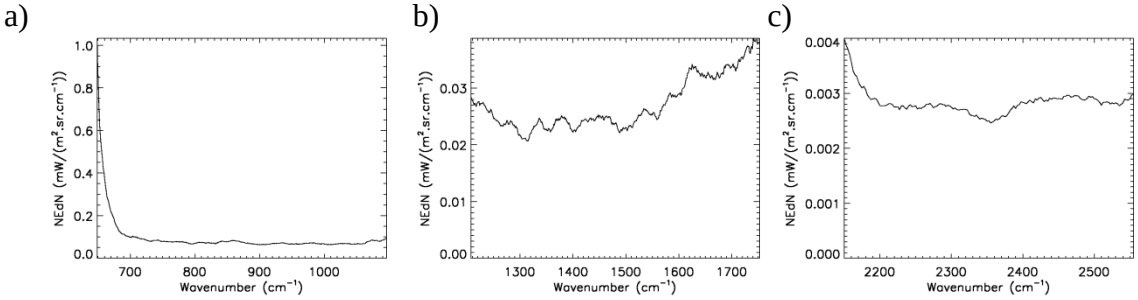

Figure 11 Example of Earth scene spectral noise estimate for FOV5, FOR 15 acquired on July 29th 2013. (a) LWIR, (b) MWIR, and (c) SWIR.

4.3.3 DS_WindowSize and ICT_WindowSize

The contents of the DS and ICT window sizes are given below:

Data field: Deep Space window size
Name: DS_WindowSize
Type: unsigned 16-bit integer
Dimension: N_{scan} x N_{dir} x N_{fov} x N_{band} (= N_g*4 x 2 x 9 x 3)
Units: Unitless
Fill value: see Table 3

Data field: ICT window size
Name: ICT_WindowSize
Type: unsigned 16-bit integer
Dimension: N_{scan} x N_{dir} x N_{fov} x N_{band} (= N_g*4 x 2 x 9 x 3)
Units: Unitless
Fill value: see Table 3

The two variables DS_WindowSize and DS_WindowSize give the number of DS and ICT spectra for calibrating the ES spectra, respectively. In order to increase the instrument background signal-noise-ration (SNR), thirty (30) DS and ICT measurements spanning 4 minutes of instrument operation are averaged per the default SDR configuration file setting. The moving window averages for DS and ICT are maintained on the uncalibrated spectrum. The normal moving average window size for CrIS calibration is 30. The moving window average is maintained by using a First-In-First-Out (FIFO) memory array. The FIFO maintains each individual contributor of the average as well as the running average. Updates to the running average are made by adding the newest contributor and subtracting the oldest contributor. Any ICT spectra, or DS spectra in the FIFO tagged as invalid are not included in the averaging.

4.3.4 ES_ZPDAmplitude and ES_ZPDFringeCount

The contents of the ES interferogram amplitude and fringe count at ZPD are given below:

Data field: Earth scene interferogram amplitude at ZPD
Name: ES_ZPDAmplitude
Type: 16-bit integer
Dimension: N_{scan} x N_{for} x N_{fov} x N_{band} (= N_g*4 x 30 x 9 x 3)
Units: Unitless
Fill value: see Table 3

Data field: Earth scene interferogram fringe count at ZPD
Name: ES_ZPDFringeCount
Type: unsigned 16-bit integer
Dimension: N_{scan} x N_{for} x N_{fov} x N_{band} (= N_g*4 x 30 x 9 x 3)
Units: Unitless
Fill value: see Table 3

ES_ZPDAmplitude represents the interferogram amplitude at ZPD for earth scene. The amplitude at ZPD of interferogram should be the maximum value of the interferogram. ES_ZPDFringCount represents the interferogram fringe count at ZPD before digital decimation. None of the interferogram sampling positions coincides exactly with the proper position of ZPD, which will introduce a linear phase in the spectral

domain. This effect is easily corrected by calibration, if it remains constant during calibration and scene measurements.

4.3.5 SdrFringeCount

The content of the Fringe Count Error count data field is given below:

Data field: Fringe Count Error counts detected in the SDR processing
Name: SdrFringeCount
Type: unsigned 16-bit integer
Dimension: N_{scan} x N_{for} x N_{fov} x N_{band} (= N_g*4 x 30 x 9 x 3)
Units: Unitless
Fill value: see Table 3

SdrFringeCount represents the fringe count error (FCE), which the calculated number of fringes that the interferogram was advanced or delayed. Once an FCE was detected, a correction to the error is attempted by the SDR FCE detection/correction algorithm. Unfortunately, as of January 2012, this FCE detection/correction algorithm was disabled.

4.3.6 ES_RDRImpulseNoise

The content of the ES RDR Impulse Noise data field is given below:

Data field: Number of samples in an ES interferogram that exceeds the impulse noise mask
Name: ES_RDRImpulseNoise
Type: unsigned 8-bit integer
Dimension: N_{scan} x N_{for} x N_{fov} x N_{band} (= N_g*4 x 30 x 9 x 3)
Units: Unitless
Fill value: see Table 3

Detection makes use of a predefined impulse noise mask, corresponding to an amplitude tight filtering window that will identify erroneous spikes. As a correction, each detected spike will be substituted by a zero count. This occurrence will be flagged for having been corrected for one or more spikes; the number of impulse noise hits is counted and reported for each interferogram via the telemetry data packets to aid in data quality assessment. This flag represents the number of samples in an interferogram that exceeded the impulse noise mask and were set to zero. The flag is a pixel level 8-bits number flag and is set for each band/FOV/FOR with a total of 6480 bits per scan.

4.3.7 MeasuredLaserWavelength, ResamplingLaserWavelength and MonitoredLaserWavelength

The contents of the three types of laser wavelength data fields are summarized below:

Data field: Metrology laser wavelength measured with neon calibration
Name: MeasuredLaserWavelength
Type: 64-bit floating point
Dimension: N_{scan} (= N_g*4)
Units: nm
Fill value: see Table 3

Data field: Wavelength for spectral re-sampling
Name: ResamplingLaserWavelength
Type: 64-bit floating point
Dimension: N_{scan} (= N_g*4)
Units: nm
Fill value: see Table 3

Data field: Monitored laser wavelength
Name: MonitoredLaserWavelength
Type: 64-bit floating point
Dimension: N_{scan} (= N_g*4)
Units: nm
Fill value: see Table 3

The laser metrology wavelength is calculated with the neon wavelength and neon fringe counts in every moving mirror sweep during the neon calibration measurements performed roughly once per orbit. The measured wavelength is the average of laser metrology wavelengths over all sweeps (30 sweeps in current setting). The resampling wavelength is the above measured wavelength divided by 2. The resampling wavelength is updated once the cumulative laser metrology wavelength change exceeds a threshold (currently set to 2 ppm) together with the update of the CMO. The monitored laser wavelength is calculated using laser diode temperature and electrical bias telemetry data. However, the temperature readings are too noisy and this feature is currently disabled.

4.3.8 DS_Symmetry

The content of the DS forward and reverse interferogram asymmetry data field is given below:

Data field: Asymmetry between the measured DS forward and reverse interferograms
Name: DS_Symmetry
Type: 64-bit floating point
Dimension: N_{scan} x N_{dir} x N_{fov} x N_{band} (= N_g*4 x 2 x 9 x 3)

Units: Unitless
Fill value: see Table 3

The variable DS_Symmetry is intended to identify the asymmetry in the measured DS interferograms. The value of this quality variable is computed using the following equation:

$$DS\_Symmetry = \frac{1}{N}\sum_{i=1}^{N}|S_{FWD}(i) - S_{REV}(i)|$$

where S_{FWD} and S_{REV} are the forward and reverse direction complex DS view interferograms, respectively, and N is the length of the interferograms.

4.3.9 DS_SpectralStability and ICT_SpectraStability

The contents of the DS and ICT spectral stability data fields are summarized below:

Data field: Spectral variability of the DS views in the moving window
Name: DS_SpectralStability
Type: 64-bit floating point
Dimension: N_{scan} x N_{dir} x N_{fov} x N_{band} (= N_g*4 x 2 x 9 x 3)
Units: Unitless
Fill value: see Table 3

Data field: Spectral variability of the ICT views in the moving window
Name: ICT_SpectralStability
Type: 64-bit floating point
Dimension: N_{scan} x N_{dir} x N_{fov} x N_{band} (= N_g*4 x 2 x 9 x 3)
Units: Unitless
Fill value: see Table 3

The two variables DS_SpectralStability and ICT_SpectralStability monitor the spectral variability of the DS and ICT view spectra within the moving window, respectively. They are calculated using the following equation:

$$SpectraStability = \frac{1}{N}\sum_{i=1}^{N}\sigma(i)$$

where N is the number of spectral bins, $\sigma(i)$ is the standard deviation of the DS or ICT radiance in the ith bin over the data samples within the moving window.

4.3.10 ICT_TemperatureStability, ICT_TemperatureConsistency and numberOfValidPRTTemperatures

The contents of the ICT temperature stability, temperature consistency and number of

valid PRT temperature data fields are summarized below:

Data field: Stability of the two ICT PRT temperature measurements
Name: ICT_TemperatureStability
Type: 32-bit floating point
Dimension: N_{scan} x N_{dir} (= N_g*4 x 2)
Units: Kelvin
Fill value: see Table 3

Data field: Consistency of the two ICT PRT temperature measurements
Name: ICT_TemperatureConsistency
Type: 32-bit floating point
Dimension: N_{scan} x N_{dir} (= N_g*4 x 2)
Units: Kelvin
Fill value: see Table 3

Data field: Number of valid PRT temperature measurements used
Name: NumberOfValidPRTTemps
Type: unsigned 8-bit integer
Dimension: N_{scan} x N_{dir} (= N_g*4 x 2)
Units: unitless
Fill value: see Table 3

ICT_TemperatureStability measures the stability of the two PRT measurements of the ICT. This variable is calculated using the following equation:

$$ICTTS = \sqrt{\sum_{i=1}^{ICTWS}\left[\bar{T}(i) - \frac{1}{ICTWS}\sum_{j=1}^{ICTWS}\bar{T}(j)\right]^2 \Big/ (ICTWS - 1)}$$

where ICTWS is the ICT Window Size, $\bar{T}(i) = \frac{1}{N}\sum_{k=1}^{N} T(i,k)$, where *T(i,k)* is the converted PRT temperature in the validated kth epoch, represents the average ICT temperature measured from a PRT for the ith scan. This variable is set separately for the two PRTs.

ICT_TemperatureConsistency measures the consistency between the two PRT measurements of the ICT. This variable is calculated using the following equation:

$$ICTTC = \frac{1}{ICTWS}\sum_{i=1}^{ICTWS}\bar{T_1}(i) - \frac{1}{ICTWS}\sum_{i=1}^{ICTWS}\bar{T_2}(i)$$

The nomenclature is similar to the ICT_TemperatureStability variable except that the subscripts 1 and 2 denote the two PRTs, respectively.

numberOfValidPRTTemperatures represents the number of PRT temperatures that have been validated using the procedure described below. The mean and standard deviation of the PRT temperatures is calculated to identify any outliers, which are defined

as being different from the mean by an amount of more than 3-sigma (standard deviation). The outliers do not enter subsequent processing.

4.4 Data Quality Flags (DQF)

A data quality flag indicates a state such as good and invalid. Some DQFs also have the state of degraded. In general, a top-level DQF has dependencies on lower level DQF and some have dependencies on data quality indicators (DQI). This section presents the various DQF. The dependency list is shown in figures for the top-level DQFs.

4.4.1 SDR scan level quality flags – QF1_SCAN_CRISSDR

The content of the QF1_SCAN_CRISSDR data field is given below:

Data field: SDR scan level quality flags
Name: QF1_SCAN_CRISSDR
Type: Unsigned 8-bit integer
Dimension: N_{scan} (= N_g*4)
Flag bit assignment: see Figure 12

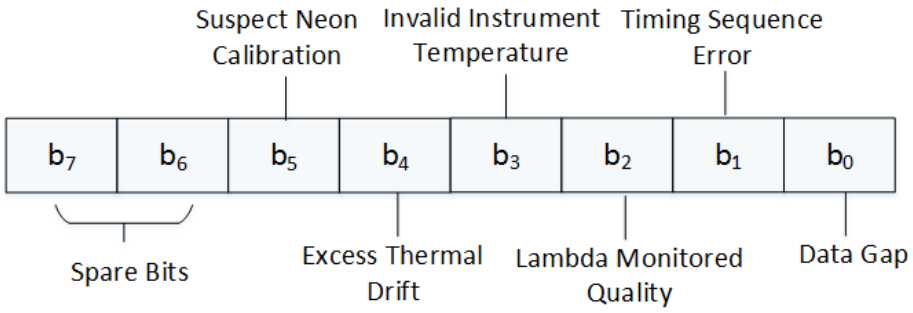

Figure 12 QF1_SCAN_CRISSDR flag bit assignment.

Flag descriptions:

Data Gap flag: value range 0-1
- 0 - No data gap
- 1 - This quality flag checks RDR data for data gaps. This flag is set if there is a data gap, i.e. missing scan(s), preceding the current scan.

Timing Sequence Error flag: value range 0-1
- 0 - No error
- 1 - This flag is set if the recorded time is not in sequence

Lambda Monitored Quality flag: value range 0-1
- 0 - Lambda Monitored calculation is valid and updated

1 - Lambda Monitored is not updated due to invalid laser diode bias current or invalid laser diode temperature

The Lambda Monitored Quality flag is intended to identify an invalid laser wavelength calculation due to invalid diode current and/or temperature measurements. This flag is set by checking if the laser diode current and temperature measurements are out of the predetermined allowable ranges.

Invalid Instrument Temperature flag: value range 0-1

0 - Valid instrument temperature
1 - Invalid instrument temperature

The Invalid Instrument Temperature flag is intended to identify the situation when the measured temperature of any instrument components (e.g., beam-splitter, scan mirror, scan baffle, etc.) are out of allowable ranges. These temperature measurements are used to compute the contributions of the instrument components to the ICT radiances.

Excess Thermal Drift flag: value range 0-1

0 - No excess thermal drift
1 - At least one of the monitored instrument temperatures has drifted more than a specified tolerance value

Suspect Neon Calibration flag: value range 0-1

0 - accepted neon calibration
1 - 25% or more of the neon calibration dataset is rejected.

4.4.2 Lunar intrusion flag – QF2_CRISSDR

The content of the QF2_CRISSDR data field is given below:

Data field: Lunar intrusion flag
Name: QF2_CRISSDR
Type: Unsigned 8-bit integer
Dimension: N_{scan} x N_{fov} x N_{band} (= N_g*4 x 9 x 3)
Flag bit assignment: see Figure 13

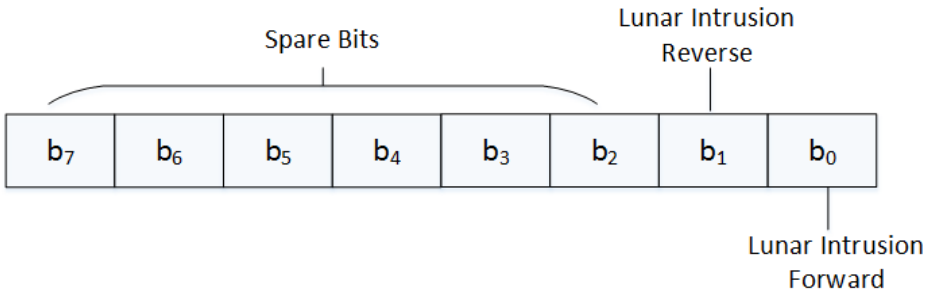

Figure 13 QF2_CRISSDR flag bit assignment.

Flag descriptions:

Lunar Intrusion Forward flag: value range 0-1

0 - No lunar intrusion
1 - At least one or more Deep Space (DS) view measurements is affected by moon in the set of DS measurements within the 30-scan moving window when the porchswing mirror has a forward sweep direction.

Lunar Intrusion Reverse flag: value range 0-1

0 - No lunar intrusion
1 - At least one or more Deep Space (DS) view measurements is affected by moon in the set of DS measurements within the 30-scan moving window when the porchswing mirror has a reverse sweep direction.

QF2_CRISSDR flags support the detection and invalidation of space reference spectra that have experienced a lunar intrusion. If lunar intrusion is detected, the new DS spectrum is marked as invalid and excluded from the moving window average. This action results in all ES spectra calibrated using the radiometric calibration where the DS sliding window average will use a lesser number of DS spectra (the current nominal DS sliding window has 30 spectra).

4.4.3 SDR Overall Quality flags – QF3_CRISSDR

The content of the QF3_CRISSDR data field is given below:

Data field: SDR overall quality flags
Name: QF3_CRISSDR
Type: Unsigned 8-bit integer
Dimension: N_{scan} x N_{for} x N_{fov} x N_{band} (= N_g*4 x 30 x 9 x 3)
Flag bit assignment: see Figure 14

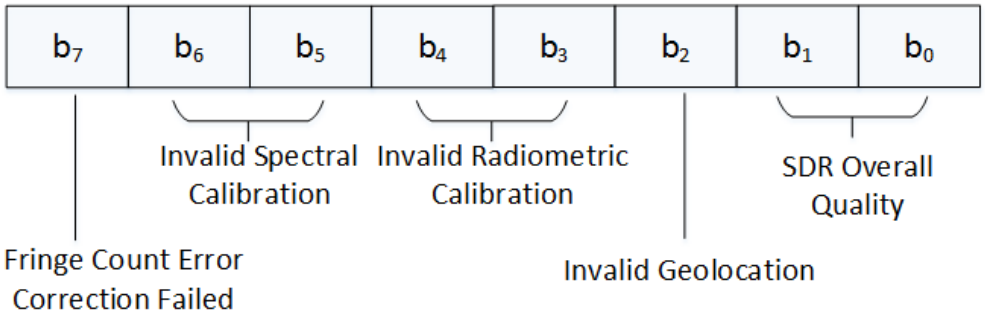

Figure 14 QF3_CRISSDR flag bit assignment.

Flag descriptions:

SDR Overall Quality flag: This is a summary flag with value range 0 – 3 where the dependency tree is shown in Figures 15 to 17.

0 - Good radiance spectrum
1 - Degraded radiance spectrum, if Invalid Geolocation flag = 1, or Invalid Radiometric Calibration flag = 1 (Degraded), or Invalided Spectral Calibration flag = 1 (Degraded)
2 - Invalid radiance spectrum, if Bit Trim Failed flag = 1, or Invalid RDR flag = 1, or RDR Fringe Count Error Detected flag = 1 (QF4 bit 2), or Invalid Radiometric Calibration flag = 2, or Invalid Spectral Calibration flag = 1, Imaginary Radiance Anomaly flag = 1, or DSWindowSize = 0, or ICTWindowSize = 0, or any channel radiance < MinRadianceThreshold, or any channel radiance > MaxRadianceThreshold,
3 - Spectrum with fill value due to Short Granule because RDR data does not exist (not missing)

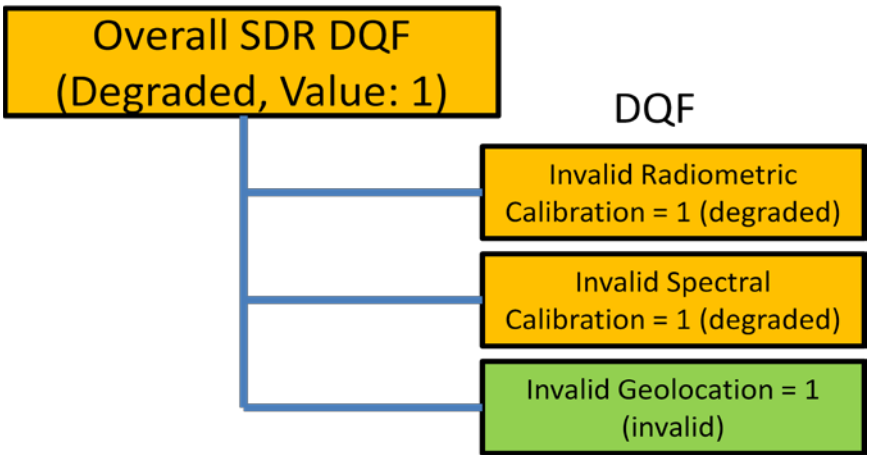

Figure 15 QF3 Overall CrIS SDR flag tree structure for degraded value 1.

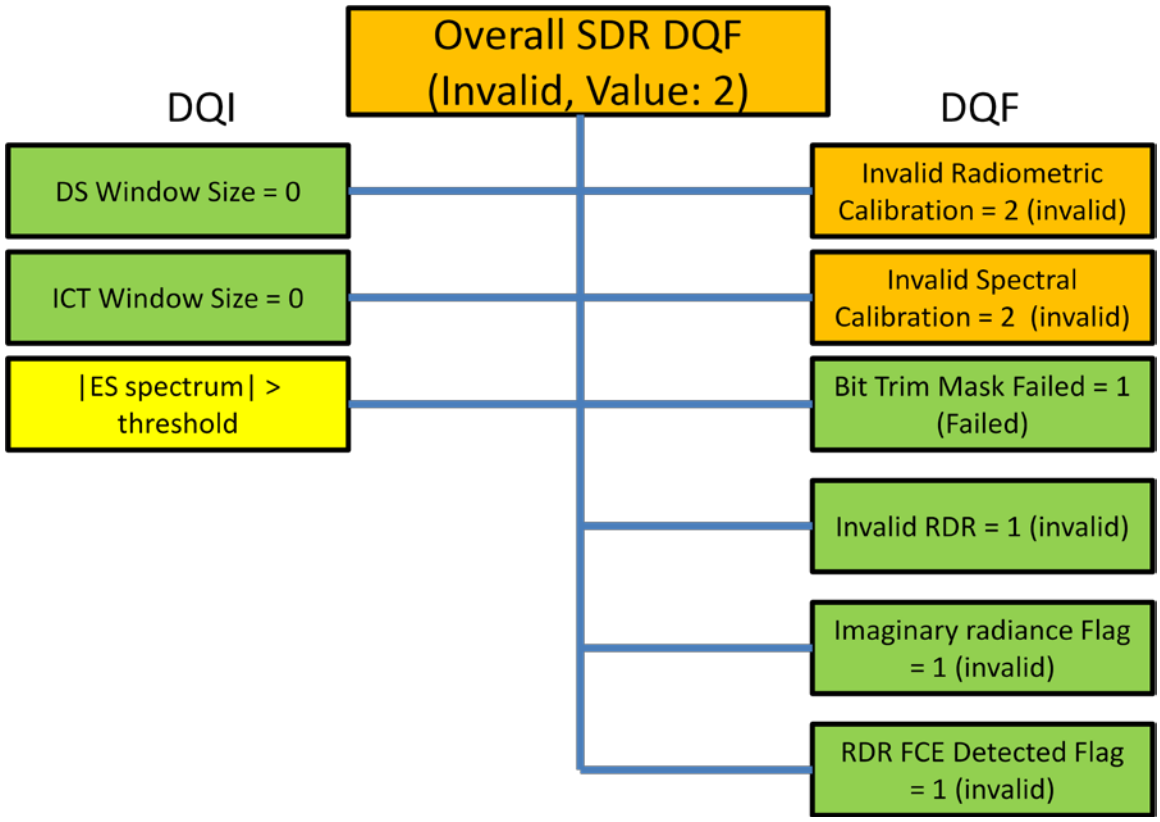

Figure 16 QF3 Overall CrIS SDR flag tree structure for invalid value 2.

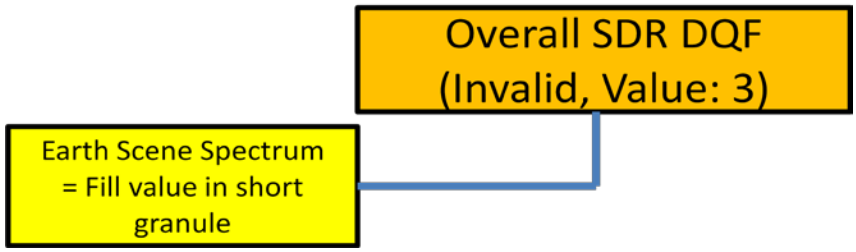

Figure 17 QF3 Overall CrIS SDR flag tree structure for invalid value 3.

Invalid Geolocation flag: value range 0 -1

0 - Good geolocation calculation
1 - Invalid geolocation calculation

Invalid Radiometric Calibration flag: value range 0-2 where the dependency tree structure is shown in Figures 18 and 19.

0 - Good radiometric calibration
1 - Degraded radiometric calibration, if 0 < DSWindowSize < Sliding Window_Size/2, or Excess Thermal Drift flag = 1, or Invalid Instrument Temperature flag = 1, or 0 < ICTWindowSize < Window_Size/2, or ICT_TemperatureStability > ICT_TemperatureStabilityThreshold, or

ICT_TemperatureConsistency > ICT_TempConsistencyThreshold, or
numberOfValidPRTTemps < numberOfValidPRTTempThreshold, or
ESRdrImpulseNoise > impulseNoiseCountThresh

2 - Invalid radiometric calibration, if DSWindowSize = 0, or ICTWindowSize = 0

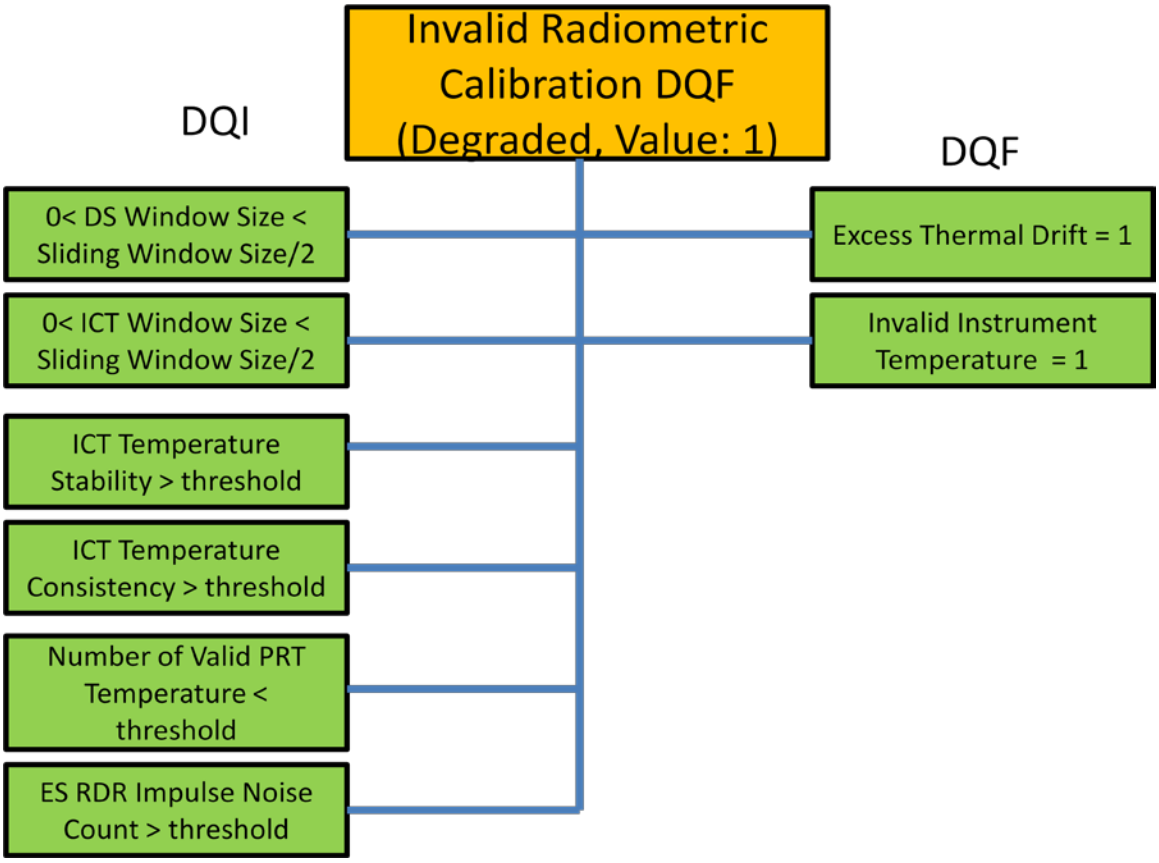

Figure 18 QF3 Invalid Radiometric Calibration flag tree structure for degraded value 1.

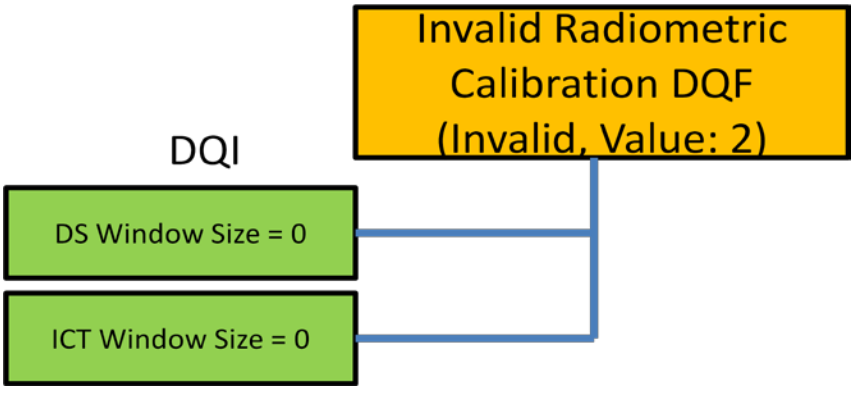

Figure 19 QF3 Invalid Radiometric Calibration flag tree structure for invalid value 2.

Invalid Spectral Calibration flag: value range 0-2 where the dependency tree structure is shown in Figures 20 and 21.

0 - Good spectral calibration
1 - Degraded spectral calibration, if Fringe Count Error Detected flag = 1, or (Suspect Neon Calibration flag = 1 and Lambda Monitored Quality flag = 0), or (Suspect Neon Calibration flag = 0 and Lambda Monitored Quality flag = 1)
2 - Invalid spectral calibration, if SDR Fringe Count Error Correction Failed flag = 1, or Suspect Neon Calibration flag = 1 and Lambda Monitored Quality flag = 1

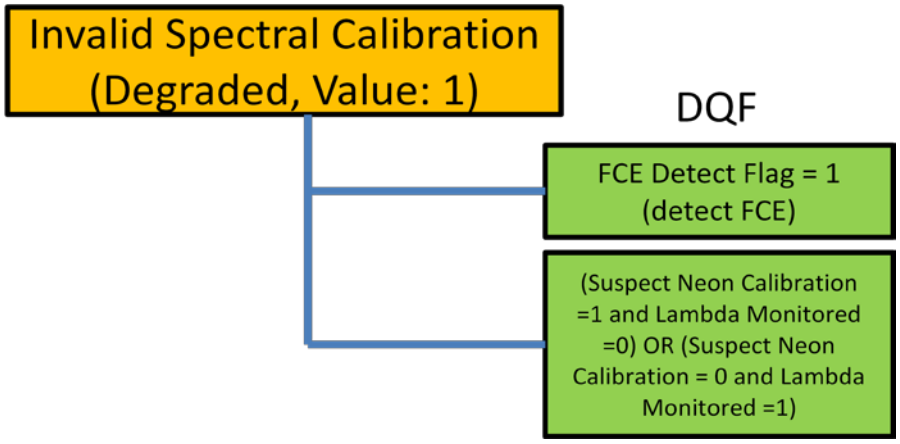

Figure 20 QF3 Invalid Spectral Calibration flag tree structure for degraded value 1.

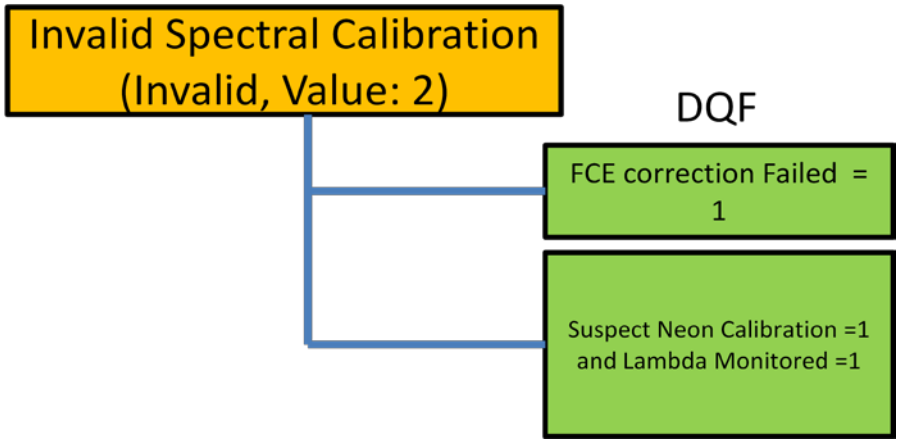

Figure 21 QF3 Invalid Spectral Calibration flag tree structure for invalid value 2.

SDR Fringe Count Error Correction Failed flag: value range 0 – 1
0 - FCE correction successful
1 - FCE correction failed

4.4.4 RDR quality flags migrated to SDR – QF4_CRISSDR

The content of the QF4_CRISSDR data field is given below:

Data field: RDR quality flags migrated to SDR

Name: QF4_CRISSDR
Type: Unsigned 8-bit integer
Dimension: N_{scan} x N_{for} x N_{fov} x N_{band} (= N_g*4 x 30 x 9 x 3)
Flag bit assignment: see Figure 22

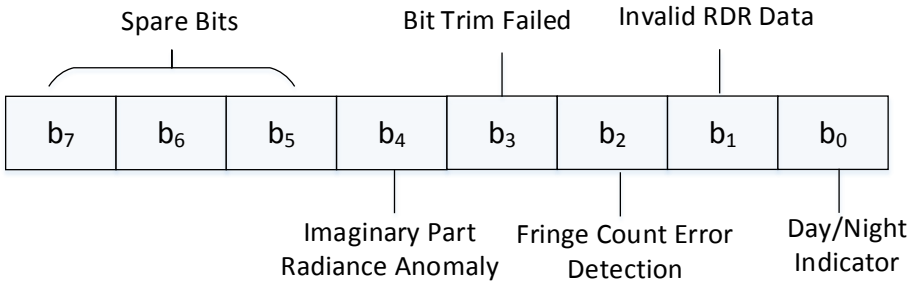

Figure 22 QF4_CRISSDR flag bit assignment.

Flag descriptions:

Day/Night Indicator flag: value range 0-1
- 0 - Day observation
- 1 - Night observation

Invalid RDR Data flag:
- 0 - Valid RDR
- 1 - The instrument exhibited operational errors and the associated interferogram(s) is excluded from SDR processing

Fringe Count Error Detected flag: value range 0-1
- 0 - No significant FCE detected
- 1 - A significant number of fringes have been missed, shifting the interferogram ZPD outside of a window monitored by the instrument, and the interferogram is excluded from SDR processing. The flag was set by the CrIS instrument and contained in the CrIS RDR data packets.

Bit Trim Failed flag: value range 0-1
- 0 - Bit Trim process successful
- 1 - RDR interferograms that were clipped during the bit trimming process and are excluded from SDR processing.

Imaginary Radiance Anomaly flag: value range 0-1

- 0 - Imaginary part of the radiance is normal
- 1 - Imaginary part radiance exceeds the threshold values, indicating anomaly in the real part of the radiance spectrum

Note that Imaginary Radiance Anomaly flag was added to QF4_CRISDR utilizing the spare bit on October 15, 2012, and it is not migrated from RDR.

4.5 CrIS SDR Radiance Metadata

The metadata field contains a host of information such as the time and aggregation of the file. For details, the relevant document is JPSS Ground Office [2011b]. It can be found at: http://www.star.nesdis.noaa.gov/jpss/ATBD.php#S772186

5. Geolocation Data

The CrIS geolocation data are computed with the CrIS geolocation algorithm, which maps the CrIS line-of-sight (LOS) pointing vectors to geodetic longitude and latitude on the Earth ellipsoid for each FOV at each scan position. Specifically, the CrIS geolocation calculation is divided into two parts, i.e. the sensor specific algorithm and the spacecraft level algorithm. The sensor specific algorithm computes CrIS LOS vectors relative to the spacecraft body frame (SBF) at given UTC time. The input data include 1) SSM in-track and cross-track servo errors, UTC time stamp, and FOR and FOV indexes from science data packets, and 2) Time stamp bias, FOR in-track (pitch) and cross-track (roll) angles relative to nadir, instrument mounting angles from each reference system, and FOV position angles from engineering data packets. The algorithm begins with FOV position angles and goes through each rotation matrices, and has the final output of the CrIS FOV LOS vectors relative to the SBF coordinate system for each FOV at each scan position.

The spacecraft level algorithm computes the intersection of those LOS vectors with the Earth ellipsoid to output geodetic longitude and latitude at given Coordinated Universal Time (UTC) time. This part of the algorithm is commonly used by all Suomi NPP instruments. The algorithm includes the following steps: 1) Transformation of the LOS vector from the Spacecraft (S/C) coordinate to the orbital coordinate using the spacecraft attitude; 2) Conversion of the LOS vector from the orbital coordinate to the Earth-centered inertial (ECI) coordinate systems based on the spacecraft's instantaneous ECI position and velocity vectors; 3) Transformation of the LOS vector from ECI to the Earth Centered Rotational coordinates (also called the Earth- Centered, Earth-Fixed (ECEF) coordinate); 4) Computation of geodetic latitude and longitude through the Earth ellipsoid intersection algorithm; and 5) Output of derived ellipsoid geolocation products, such as solar and sensor azimuth and zenith angles as well as the sensor range. The algorithm is described in the Joint Polar Satellite System (JPSS) Operational Algorithm Description (OAD) Document for Common Geolocation Software [*JPSS Configuration Management Office*, 2012a] and VIIRS geolocation ATBD [*JPSS Configuration Management Office*, 2012b].

CrIS has three bands and each band has a focal plane. Only the detector position angles from the LWIR band are used for geolocation computation. The radial offsets of all 27 CrIS detectors from the interferometer axis are determined using the relative spectral calibration of these FOVs. The spatial offsets (or co-registration) of focal plane detectors between the LWIR and the MWIR/SWIR bands derived from relative

frequency calibration can be used to connect the LW geolocation to the other two focal planes. The detector co-registration difference between the LWIR and either the MWIR or SWIR focal planes is well within the 1.4% co-registration specification for CrIS focal planes.

In the following sections, the variables in the HDF5 file are located under "All_Data.CrIS-SDR-GEO_ALL" structure.

5.1 FOV Latitude and Longitude

The contents of the FOV latitude and longitude data fields are summarized below:

Data field: FOV latitude; FOV longitude
Names: Latitude; Longitude
Type: 32-bit floating point
Dimension: N_{scan} x N_{for} x N_{fov} (= N_g*4 x 30 x 9)
Units: degree
Fill value: see Table 3

Latitude identifies the north to south location of a point on the Earth. Latitude is defined precisely as the angle between the vertical at a location, and the equatorial plane of the Earth. In the CrIS geolocation dataset, latitude 0° at the Equator, +90° at the north pole, and -90° at the south pole. Longitude identifies the east to west location of a point on the Earth, by measuring the angular distance from the Greenwich meridian (or Prime meridian, where longitude is 0), along the equator. The values range from -180° to 180° and the positive values indicates the East direction.

5.2 FOR time, Start time and Mid-time

The data field contents of the FOR observation time, the beginning time of a scan and the mid-time of a scan are summarized below:

Data field: FOR observation time
Name: FORTime
Type: 64-bit integer
Dimension: N_{scan} x N_{for} (= N_g*4 x 30)
Units: micro-second since 1/1/1958 (IET time)
Fill value: see Table 3

Data field: Scan start time
Name: StartTime
Type: 64-bit integer
Dimension: N_{scan} (= N_g*4)

Units: micro-second since 1/1/1958 (IET time)
Fill value: see Table 3

Data field: Mid time of a scan
Name: MidTime
Type: 64-bit integer
Dimension: N_{scan} (= N_g*4)
Units: micro-second since 1/1/1958 (IET time)
Fill value: see Table 3

5.3 FOV Satellite Zenith and Azimuth Angles

The contents of the FOV satellite zenith and azimuth angle data fields are summarized below:

Data fields: FOV satellite zenith angle; FOV satellite azimuth angle
Names: SatelliteZenithAngle; SatelliteAzimuthAngle
Type: 32-bit floating point
Dimension: N_{scan} x N_{for} x N_{fov} (= N_g*4 x 30 x 9)
Units: degree
Fill value: see Table 3

Satellite zenith defines the angle between a straight line from a given geolocated FOV center on the earth's surface to the satellite and a line from the same point on the earth's surface that is perpendicular to the earth's surface at that point (the zenith point). The satellite zenith angle ranges from 0° to 90°. Figure 23 explains the definition of the satellite zenith angle. The satellite azimuth angle is the angle formed between a reference direction (North) and a line from the geolocated FOV center to a point of satellite projected on the same plane that contains the reference direction (measured clockwise positive from North). The values range from -180° to 180°. The 90° indicates the East direction while -90 ° represents the West direction. The angle represented by the red curved arrow in Figure 24 is an example of the satellite azimuth angle.

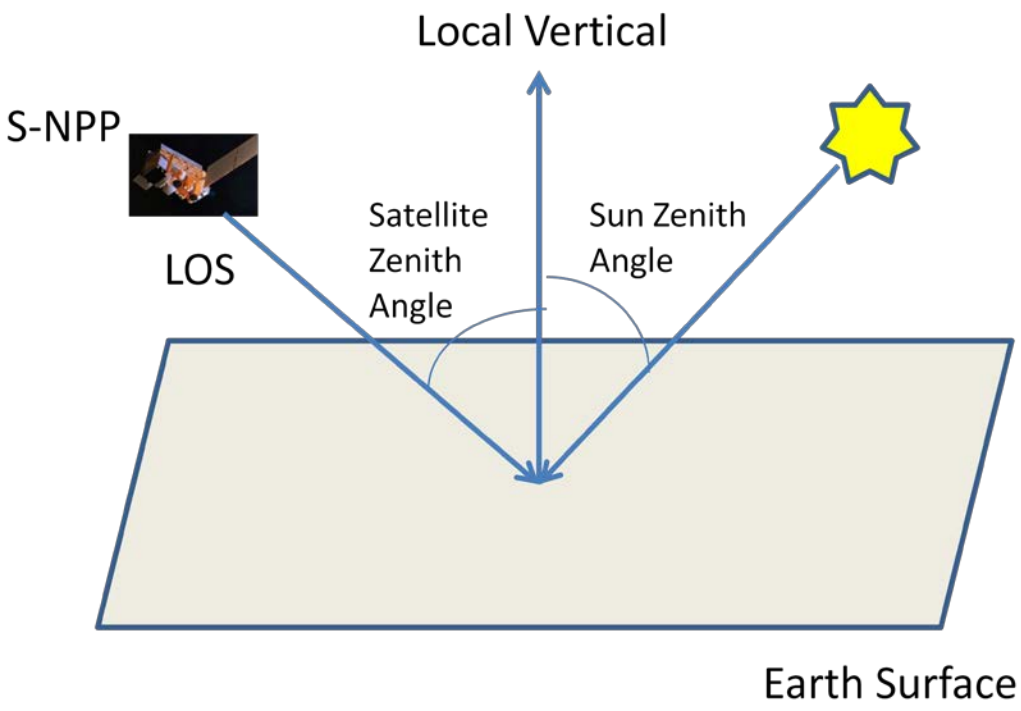

Figure 23 Schematic representation of the satellite and solar zenith angles.

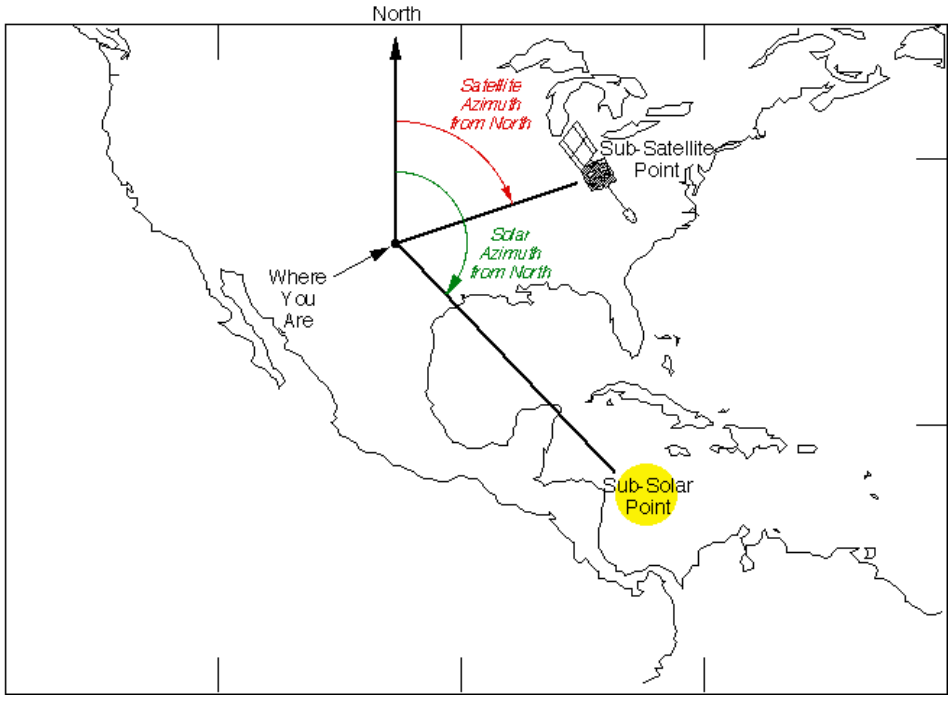

Figure 24 Definition of the satellite and solar azimuth angles.

[from **http://science-edu.larc.nasa.gov/SCOOL/definitions.html**].

5.4 FOV solar Zenith and Azimuth Angles

The contents of the FOV solar zenith and azimuth angle data fields are summarized below:

Data fields: FOV solar zenith angle; FOV solar azimuth angle
Names: SolarZenithAngle; SolarAzimuthAngle
Type: 32-bit floating point
Dimension: N_{scan} x N_{for} x N_{fov} (= N_g*4 x 30 x 9)
Units: degree
Fill value: see Table 3

Solar zenith angle is the angle measured at the earth's surface between the sun and the zenith. The sun zenith angle ranges from -90° to 90°. The negative angles indicate that the Sun is below the Horizon. Figure 23 explains the definition of the solar zenith angle. The solar azimuth is the angle formed between a reference direction (North) and a line from the observer to a point of the sun projected on the same plane that contains the reference direction (measured clockwise positive from North). The values range from -180° to 180°. The 90° indicates the East direction and -90 ° the West direction. The angle represented by the green curved arrow in Figure 24 is an example of the solar azimuth angle.

5.5 Ellipsoid-Geoid Separation - Height

The content of the FOV Ellipsoid-Geoid separation height data field is summarized below:

Data field: Ellipsoid-Geoid separation height
Name: Height
Type: 32-bit floating point
Dimension: N_{scan} x N_{for} x N_{fov} (= N_g*4 x 30 x 9)
Units: meter
Fill value: see Table 3

The Geoid is the gravitational equipotential surface that is best approximated by the mean sea surface of the ocean in the absence of other influences such as winds, solid and oceanic tides, and oceanic current dynamic topography. All points on that surface have the same scalar potential. The local gravitational acceleration direction is perpendicular to the geoid at all points. Deformation of the Geoid is mainly due to uneven distribution of mass. Geodetic data define the size and shape of the earth and the origin and orientation of the coordinate systems used to map the Earth. The reference ellipsoid is usually

defined by the semi-major (equatorial radius) and the flattening (the relationship between equatorial and polar radii). The World Gravity Solution WGS 84 datum surface, used in the GrIS geolocation data, is an oblate spheroid (ellipsoid) with major (equatorial) radius a = 6378137 m at the equator and flattening f = 1/298.257223563. The polar semi-minor axis b then equals a times (1−f), or 6356752.3142 m. The Ellipsoid-Geoid separation height represents the distance between Ellipsoid (green curve in Figure 25) and Geoid (red curve) with the unit of meter for each geolocated FOV center (the red arrow N in Figure 25).

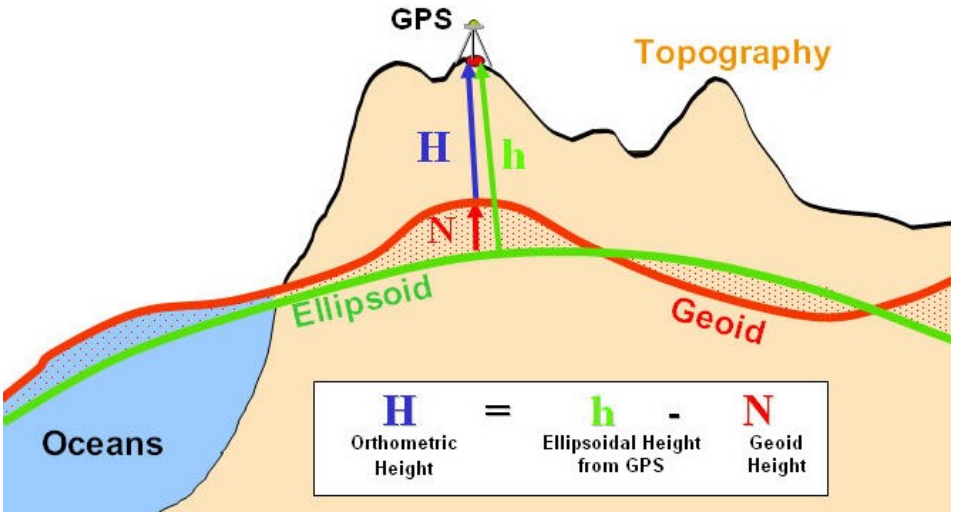

Figure 25 Illustration of the Earth ellipsoid and the geoid separation.
[from **http://principles.ou.edu/earth_figure_gravity/geoid/**]

5.6 Line of Sight Distance – SatelliteRange

The content of the FOV satellite range data field is summarized below:

Data field: Line of sight distance from the ellipsoid intersection to the satellite
Name: SatelliteRange
Type: 32-bit floating point
Dimension: N_{scan} x N_{for} x N_{fov} (= N_g*4 x 30 x 9)
Units: meter
Fill value: see Table 3

Referring to the equation below, the satellite position is the point $\vec{P}$, the line-of-sight (LOS) unit exit vector is $\vec{L}$, and the intersection of the LOS with the Earth ellipsoid is the

geolocated point $\vec{G}$ in the ECI frame.The satellite slant range λ is the distance from the satellite position $\vec{P}$ to geolocated point $\vec{G}$ with the unit of meters. Figure 26 shows the satellite slant range with respect to the satellite and the geolocated points.

$$\vec{G} = \vec{P} + \lambda\vec{L}$$

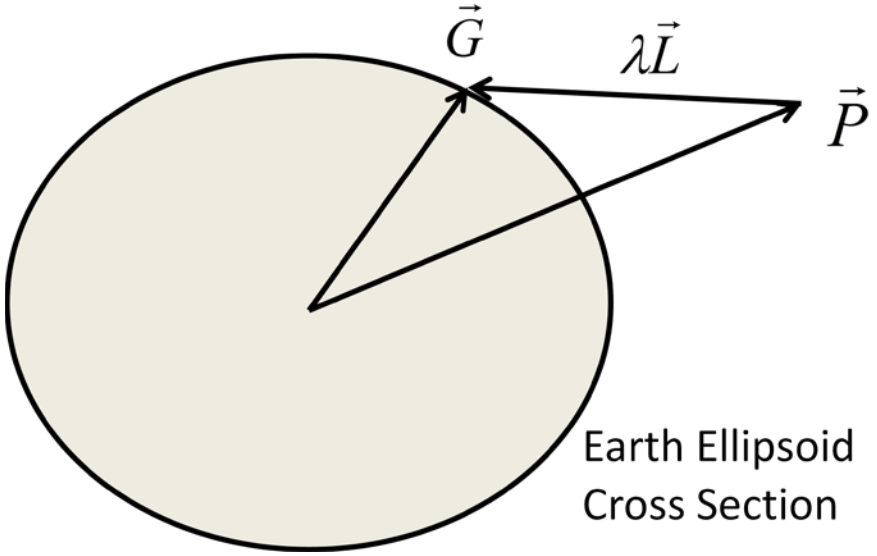

Figure 26 Illustration of spacecraft position and satellite range in ECI.

5.7 Spacecraft Position, Attitude and Velocity

The contents of the spacecraft position, attitude and velocity data fields are summarized below:

Data field: Spacecraft position
Name: SCPosition
Type: 32-bit floating point
Dimension: N_{scan} x $N_{s/c}$ (= N_g*4 x 3)
Units: meter
Fill value: see Table 3

Data field: Spacecraft attitude
Name: SCAttitude
Type: 32-bit floating point
Dimension: N_{scan} x $N_{s/c}$ (= N_g*4 x 3)

Units: arcsecond
Fill value: see Table 3

Data field: Spacecraft velocity
Name: SCVelocity
Type: 32-bit floating point
Dimension: N_{scan} x $N_{s/c}$ (= N_g*4 x 3)
Units: m/s
Fill value: see Table 3

The Earth-Centered Inertial (ECI) system of coordinate has its origin located at the center mass of the Earth. In particular, one of commonly used ECI frames is defined with the Earth's Mean Equator and Equinox at 12:00 Terrestrial Time on 1 January 2000 (J2000 ECI). The Earth Centered Rotational (ECR) coordinate is the ECI adjusted for the Earth rotation, nutation, and precession in addition to the polar wander. The fields of spacecraft position represent the spacecraft position in ECR at the mid-time of a scan as (x, y, z) in a unit of meter as shown in Figure 27. The spacecraft velocity in the ECR Coordinate is (dx/dt, dy/dt, dz/dt) at the mid-time of a scan with a unit of meter per second.

The SCAttitude information gives the transformation from the spacecraft body frame in the J200 ECI coordinates at the mid-scan time to the orbital frame. The SCAttitude is a 2-D array and has the dimension [Ng*4, 3]. The second column has 3 reported angles with units in arcseconds that are the yaw [Ng*4, 0], the pitch [Ng*4, 1], and the roll [Ng*4, 2]. Using the spacecraft frame of the fixed coordinate system, the pitch angle is a space rotation around the spacecraft (S/C) y-axis, followed by a space rotation of the roll angle around the S/C x-axis, then followed by a space rotation of the yaw angle around the S/C z-axis. Detailed information on the ECI and spacecraft system of coordinates is found in [JPSS Configuration Management Office, 2011c].

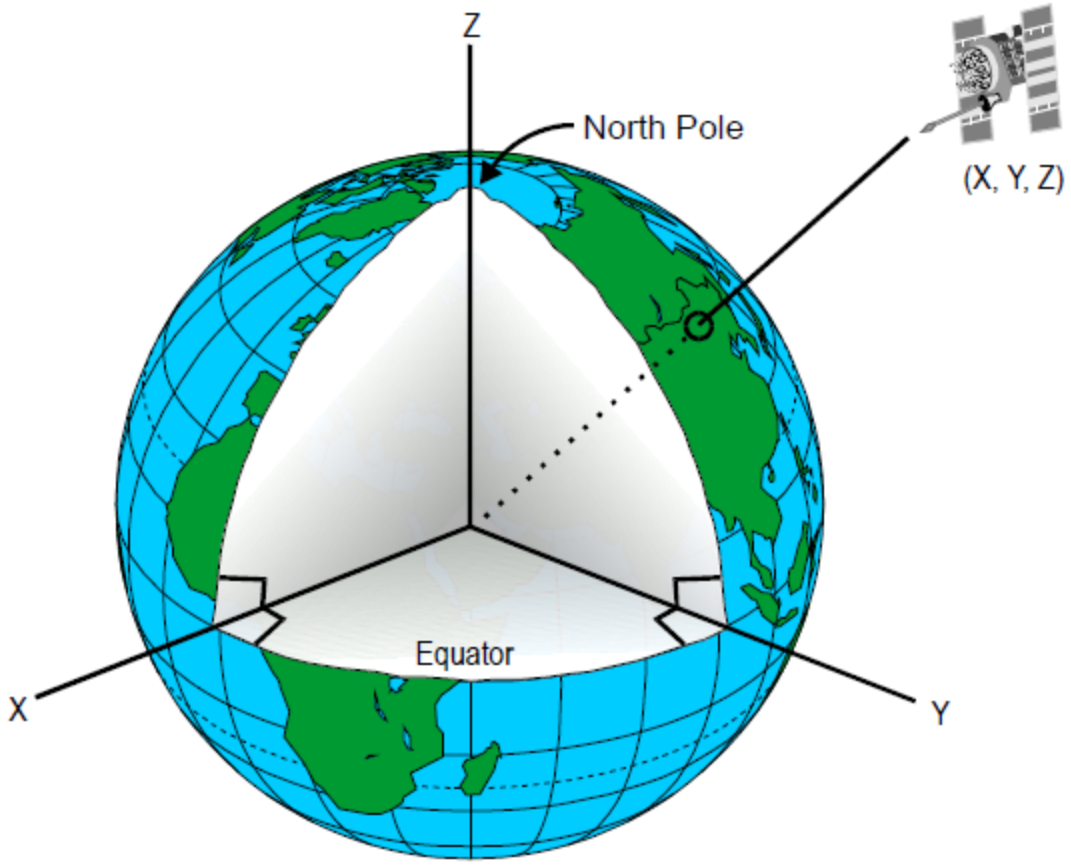

Figure 27 Satellite position in the Earth Centered Inertial (ECI) system of coordinates (from **http://upload.wikimedia.org/wikipedia/commons/3/32/Earth_Centered_Inertial_Coordinate_System.png)**

5.8 Geolocation quality flags - QF1_CRISSDRGEO

The content of the geolocation quality flag QF1_CRISSDRGEO data field is given below:

Data field: Geolocation quality flags
Name: QF1_CRISSSDRGEO
Type: Unsigned 8-bit integer
Dimension: N_{scan} (=N_g*4)
Flag bit assignment: see Figure 28

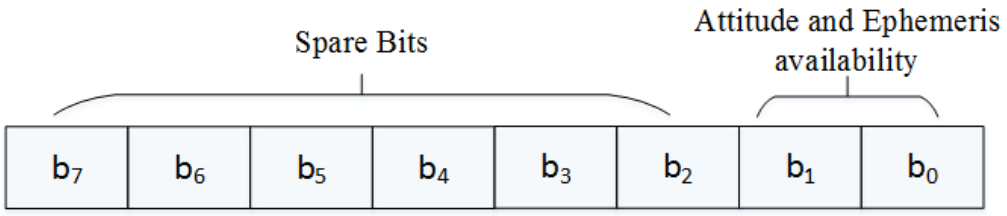

Figure 28 CRSSDR Geolocation flag bit representation.

Flag descriptions:

Attitude and Ephemeris availability: value range 0-3

0 - Normal (Attitude and Ephemeris available)
1 - Missing data <= Small_Gap
2 - Small_Gap < Missing data < Granule Boundary
3 - Missing Data >= Granule Boundary

Note that the Geolocation Invalid Geolocation quality flag is stored in the SDR quality flag variable QF3_CRISSDR.

5.9 Geolocation Metadata Information

The metadata field contains a host of information about the time and aggregation of the file. The CrIS SDR geolocation file contains over 30 parameters. The time stamp field are in UTC whereas the so-called IET is the number of microseconds passed the epoch time of January 1st 1958 at 0H:0M:0S. For details, the relevant document is JPSS Ground Office [2011b]. It can be found at:

http://www.star.nesdis.noaa.gov/jpss/ATBD.php#S772186

6. References

The main sources that may be of direct interest and utility to the SDR users are the Algorithm CrIS SDR Theoretical Basis Documents (ATBD) for processing algorithms, calibration, geolocation, and common data format control which are readily available from the JPSS website at http://www.star.nesdis.noaa.gov/jpss. Users may find the following documents particularly useful:

1. Chen, Y., Y. Han and F. Weng (2013)**,** Detection of Earth-rotation Doppler Shift from Suomi National Polar-Orbiting Partnership Cross-track Infrared Sounder. Appl. Opt., 52, 6250–6257.
2. Han, Y., et al. (2013), Suomi NPP CrIS measurements, sensor data record algorithm, calibration and validation activities, and record data quality, J. Geophys. Res. Atmos., 118, *doi:*10.1002/2013JD020344.
3. JPSS Configuration Management Office (2011a), Joint Polar Satellite System (JPSS) Cross Track Infrared Sounder (CrIS) Sensor Data Records (SDR) algorithm theoretical basis document (ATBD), JPSS office, document code 474: 474-00032, October 2011. [Available online at http://www.star.nesdis.noaa.gov/jpss/ATBD.php#S796056].
4. JPSS Configuration Management Office (2011b), Joint Polar Satellite System (JPSS) Common Data Format Control Book- External, Volume III - SDR/TDR Formats, document code 474-00001-03, August 13th 2011, available online at http://www.star.nesdis.noaa.gov/jpss/ATBD.php#S772186
5. JPSS Configuration Management Office (2011c), Joint Polar Satellite System (JPSS) VIIRS Geolocation Algorithm Theoretical Basis Document (ATBD), document code 474-00053, July 31st 2011, available online at http://www.star.nesdis.noaa.gov/jpss/ATBD.php#S470396.
6. Strow, L. L., H. Motteler, D. Tobin, H. Revercomb, S. Hannon, H. Buijs, J. Predina, L. Suwinski, and R. Glumb (2013), Spectral calibration and validation of the Cross–track Infrared Sounder (CrIS) on the Suomi NPP satellite, J. Geophys. Res. Atmos., 118, doi:10.1002/2013JD020480.
7. Tobin, D., et al. (2013), Suomi-NPP CrIS radiometric calibration uncertainty, J. Geophys. Res. Atmos., 118, 10,589–10,600, *doi:*10.1002/jgrd.50809.
8. Wang, L., D. A. Tremblay, Y. Han, M. Esplin, D. E. Hagan, J. Predina, L. Suwinski, X. Jin, and Y. Chen (2013), Geolocation assessment for CrIS sensor data records, J. Geophys. Res. Atmos., 118, doi:10.1002/2013JD020376.
9. Zavyalov, V., M. Esplin, D. Scott, B. Esplin, G. Bingham, E. Hoffman, C. Lietzke, J. Predina, R. Frain, L. Suwinski, Y. Han, C. Major, B. Graham, L. Phillips (2013), Noise performance of the CrIS instrument, J. Geophys. Res., doi: 10.1002/2013JD020457.

7. Acknowledgements

The authors would like to thank Dr Lihang Zhou, Tony Reale, and Dave Johnson for their critical review, comments, and suggestions for this manuscript. Thanks are extended to all CrIS SDR and EDR team members for their hard work validating and ensuring the CrIS SDR data quality. Funding for this work was provided by the NOAA JPSS program. The manuscript contents are solely the opinions of the authors and do not constitute a statement of policy, decision, or position on behalf of NOAA or the U.S. government.

NOAA SCIENTIFIC AND TECHNICAL PUBLICATIONS

The National Oceanic and Atmospheric Administration **was established as part of the Department of Commerce on October 3, 1970. The mission responsibilities of NOAA are to assess the socioeconomic impact of natural and technological changes in the environment and to monitor and predict the state of the solid Earth, the oceans and their living resources, the atmosphere, and the space environment of the Earth.**

The major components of NOAA regularly produce various types of scientific and technical information in the following types of publications

PROFESSIONAL PAPERS – Important definitive research results, major techniques, and special investigations.

CONTRACT AND GRANT REPORTS – Reports prepared by contractors or grantees under NOAA sponsorship.

ATLAS – Presentation of analyzed data generally in the form of maps showing distribution of rainfall, chemical and physical conditions of oceans and atmosphere, distribution of fishes and marine mammals, ionospheric conditions, etc.

TECHNICAL SERVICE PUBLICATIONS – Reports containing data, observations, instructions, etc. A partial listing includes data serials; prediction and outlook periodicals; technical manuals, training papers, planning reports, and information serials; and miscellaneous technical publications.

TECHNICAL REPORTS – Journal quality with extensive details, mathematical developments, or data listings.

TECHNICAL MEMORANDUMS – Reports of preliminary, partial, or negative research or technology results, interim instructions, and the like.

U.S. DEPARTMENT OF COMMERCE
National Oceanic and Atmospheric Administration
National Environmental Satellite, Data, and Information Service
Washington, D.C. 20233